CHAPTER 2

BIOASSAY GUIDED FRACTIONATION OF THE CRUDE EXTRACT FROM *CROTON STEENKAMPIANUS*

CHAPTER 2

BIOASSAY GUIDED FRACTIONATION OF THE CRUDE EXTRACT FROM *CROTON STEENKAMPIANUS*

2.1 Introduction

Plants from the Euphorbiaceae family are well known for their medicinal properties and are used to treat many diseases around the world (Suarez *et al.,* 2003). This family has about 300 genera and 5 000 species of trees, shrubs and herbs. The genus *Croton* has about 750 species of trees, shrubs and herbs distributed in tropical and subtropical regions and is rich in constituents with biological activity (Suarez *et al.,* 2003). This genus is being used to treat malaria, hepatic and kidney disorders, obesity, hypertension, wounds, inflammation, tumors, diabetes, diarrhoeas, rheumatism, gastric ulcers and pain. A number of biologically active compounds (terpenes, flavonoids and alkaloids) have been isolated from it (Silva *et al.,* 2005; Suarez *et al.,* 2003; Suarez *et al.,* 2006; Ngadjui *et al.,* 2002).

Before 2004, *C. steenkampianus* had no history of medicinal usage or any record of the isolation of an active compound. However, it has since been reported that the crude extracts from the leaves showed antiplasmodial activity and contained several interesting compounds such as a diterpene with a new exoskeleton, one triterpene and two flavonoids (Prozesky 2004). Antibacterial activity was used to guide the isolation of compounds from fractions because it is simpler and quicker to perform. This method is supported by the fact that most compounds showing antibacterial activity also show antiplasmodial activity (Boonphong *et al*., 2007; Zdzislawa, 2007).

2.2 Materials and Methods

2.2.1 Collection of plant materials

Leaves of *C. steenkampianus* Gerstner were collected in April 2003, at Thembe Elephant Park in northern KwaZulu-Natal, South Africa, and a voucher specimen (registry number 92520) is preserved at the HGWJ Schweickerdt Herbarium (PRU) at the University of Pretoria.

2.2.2 Methods

2.2.2.1 Preparation of the crude extract

The leaves were allowed to dry for two weeks at room temperature. The dried leaves (2 kg) were then crushed to a powder and extracted with ethanol at room temperature for 3 days. The resulting mixture was then filtered under vacuum and the residue generated was extracted further with ethanol. The combined filtrate was evaporated under reduced pressure at 37°C to yield an 80 g total extract.

2.2.2.2 Bacterial culturing and antibacterial testing

Bacillus cereus and *Escherichia coli* were obtained from the Department of Microbiology and Plant Pathology, University of Pretoria. These bacteria were maintained on nutrient agar slant and were recovered for testing by culturing them in a nutrient broth. A sterile loop was used to transfer some bacterial colonies to the nutrient broth (50 ml) in conical flasks under sterile conditions (in a laminar flow cabinet). The opening of the flask was then plugged with cotton wool, covered with aluminium foil, placed on a shaker and incubated for 24 hours at 37°C. After 24 hours, the bacterial culture was centrifuged at 3 000 rpm for 20 minutes. The supernatant was discarded and the sedimented bacteria resuspended in fresh nutrient broth (Lund and Lyon, 1975).

The isolation of the possible antiplasmodial active fraction and compound was guided by antibacterial testing using direct bioautography on TLC plates. This is because the bioassay is simpler and quicker to perform than an antiplasmodial bioassay and most compounds showing antibacterial activity also show antiplasmodial activity (Boonphong, 2007; Zdzislawa, 2007). The extract or fraction (~5 µl) was applied to silica gel 60 plates (Merck), developed in 3-10% methanol in chloroform and observed under ultraviolet light (254 and 366 nm). The developed TLC plate was then left to dry overnight (for the solvent to evaporate completely). It was then sprayed with bacterial suspension until it appeared translucent and incubated at 25°C for 24 hours in humid conditions. The plates were then sprayed with an aqueous solution of 2.0 mg/ml p-iodonitrotetrazolium violet (Sigma) and reincubated at

25°C for 3 hours. Any inhibition of bacterial growth could be clearly seen as white spots on a red background (Begue and Kline, 1972; Eloff, 1998).

2.2.2.3 Isolation and identification of compounds

The total ethanol extract (80 g) was applied (Fig. 2.1) to a flash silica gel column (10 x 50 cm). The column was developed with a solvent gradient of hexane : ethyl acetate, in order of increasing polarity (100:0 to 0:100) and the fractions were collected. Similar fractions were pooled together according to the TLC profile to yield 4 fractions, which was then tested for antibacterial activity. Fractions 2 and 4 showed antibacterial activity.

Fraction 2 (10 g) was applied to a flash silica gel column (3.0 x 50 cm) and eluted with solvent gradient of hexane : ethyl acetate mixture (95:5 to 90:10). Similar fractions obtained were pooled together resulting in six main fractions (2.1-2.6) while 2.4 to 2.6 showed antibacterial activity.

Fraction 2.5 (2.4 g) was applied to a flash silica gel column (2.5 x 30 cm), and eluted with a solvent gradient of hexane : ethyl acetate in a 95:5 to 90:10. Sub-fraction 2.5.13 that showed antibacterial activity was purified further with a Sephadex LH-20 column, using methanol as eluent to yield the pure compound **1** (100 mg).

Fraction 2.6 (2.4 g) was further purified on a silica column. A solvent mixture of hexane : ethyl acetate was applied to the column in a 1:19 to 1:1 ratio. Sub-fraction 2.6.4 was further purified with a Sephadex LH-20 column with methanol as eluent to yield compound **1** (48 mg) and eriodictyol (5 mg).

Fraction 2.4, upon standing overnight, gave a crystalline compound which was washed with hexane : ethyl acetate (1:1) to give compound **2** (150 mg). The remaining part of fraction 2.4 was further purified with a flash silica gel column (2.5 x 30 cm) which was developed with a solvent system of hexane : ethyl acetate in ratio 7:3 (100 ml fractions collected), to yield more of the pure compound **2** (100 mg).

Fraction 4 (5 g) was applied to a flash silica gel column (3.0 x 50 cm) and developed with a solvent gradient of hexane : ethyl acetate in a 95:5 to 90:10. Sub-fraction 4.2 that showed antibacterial was further purified with a Sephadex LH-20 column, which was developed with solvent mixture methanol : chloroform mixture (1:9) to yield tamarixetin (5 mg) and quercetin (10 mg) respectively. Fraction 4.2.1 showed antibacterial activity and was purified further on a silica gel column (2.5 x 30 cm) and eluted with a solvent mixture of methanol : chloroform (1:19). The resulting sub-fraction 4.2.1.4 which still indicated antibacterial activity was then purified further with a Sephadex LH-20 column and eluted with water : ethanol mixture (1:19) to yield the pure compound **3** (50 mg).

2.2.2.4 Structure elucidation

The isolated compounds were identified by their proton-nuclear magnetic resonance (^{1}H-NMR), carbon-nuclear magnetic (^{13}C-NMR), two dimensional NMR, mass spectroscopy (MS), infra red (IR), UV spectra and X-ray crystallography (Fig. 2.5-2.8) (section 2.3). The nuclear magnetic resonance (NMR) data were obtained at 300 MHz on a Bruker ARX 300 NMR spectrometer using $CDCl_3$ as solvent with tetramethylsilane (TMS) as internal standard.

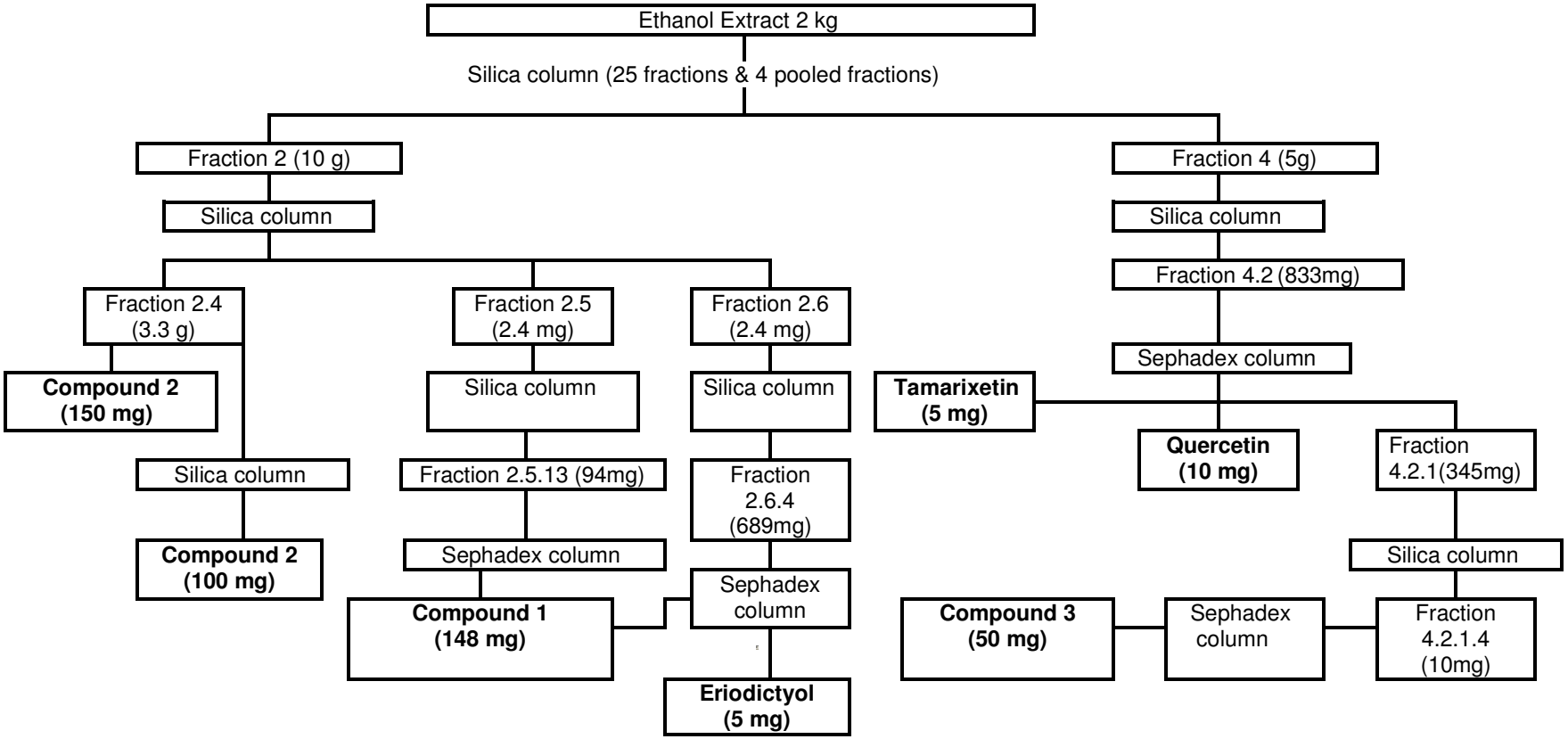

Figure 2.1: Schematic representation of the bioassay guided isolation of active compounds from *C. steenkampianus.* Only fractions with antibacterial activity are shown.

2.3 Results and Discussion

Fractions with antibacterial activity have been reported to show antiplasmodial activity (Prozesky, 2004; Boonphong *et al.,* 2007; Zdzislawa, 2007). Therefore, antibacterial-guided fractionation was used to monitor and direct the isolation of compounds with possible antiplasmodial activity from the crude ethanol extracts of the leaves of *C. steenkampianus*. Pooled fractions from the columns were then collected and tested against *Bacillus cereus*. A typical result of this method is shown in Fig. 2.2 and 2.3. This method has led to the isolation of six compounds: two diterpenes with new skeletons, three flavonoids and one indane (Fig. 2.4). Compounds showed moderate to good antibacterial activity. The antibacterial activity observed in fractions (Fig. 2.2b) is more pronounced than those of pure compounds (Fig. 2.3). This could be due to other compounds not isolated having synergistic effects in the fractions.

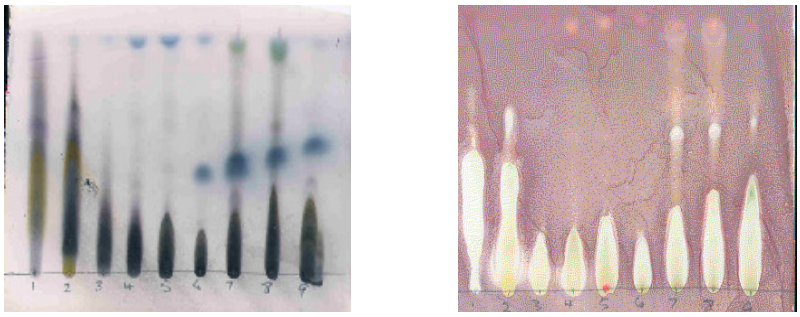

(a) **(b)**

Figure 2.2: Typical results obtained from the pooled fractions from the silica column tested for antibacterial activity. Both TLC plates were developed with chloroform : methanol (9:1). The white zones on TLC plate (b) indicate antibacterial activity.

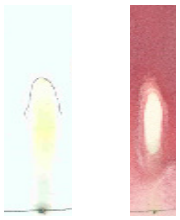

(1a) (1b)

Purified fraction of the indane.

(2a) (2b)

Purified fraction of quercetin.

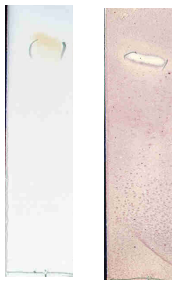

(3a) (3b)

Purified fraction of tamarixetin.

Figure 2.3: TLC plates showing antibacterial activity of pure compounds. The TLC for the purified fractions were developed in solvent mixture: hexane : ethyl acetate (1:1) for indane, chloroform : methanol (9:1) for quercetin and tamarixetin. a) sprayed with vanillin reagent. b) the white zone indicates antibacterial activity.

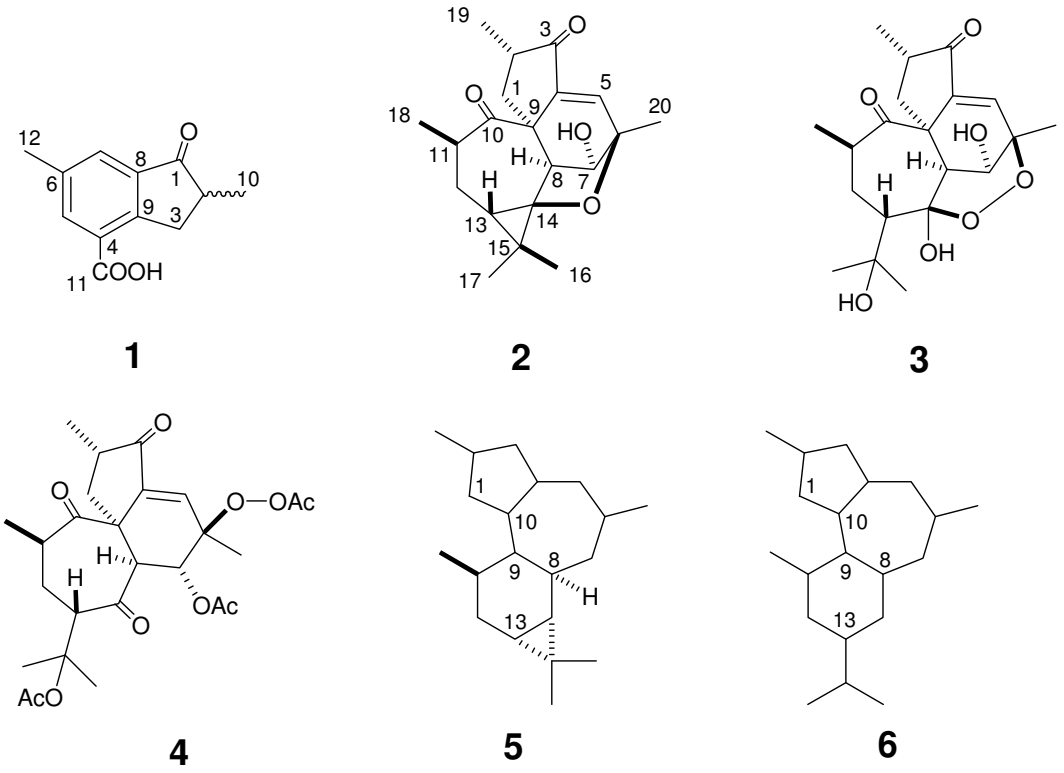

Figure 2.4: Structures of isolated compounds.

2,6-Dimethyl-1-oxo-4-indanecarboxylic acid (**1**) was isolated as a amorphous white solid, it showed in UV (MeOH) spectra absorptions at λ_{max} 215, 248, 310 nm, the IR (KBr) showed absorption peaks at $_{max}$ 3400-2300, 2924, 1709, 1580, 1459, 1423, 1250, 1182, 1133, 927, 836, 693 cm^{-1}. Low-resolution mass spectrometry and combustion analysis indicated a molecular formula $C_{12}H_{12}O_3$ for **1** and its NMR spectroscopic data (Table 2.1) were in agreement with a structure of 2,6-dimethyl-1-oxo-4-indanecarboxylic acid. In particular, the HMBC (Fig. 2.13) correlations observed for **1** (C-1 with H-2, H_2-3, H-7, and Me-10; C-12 with H-5 and H-7; C-9 with H-2, H_2-3, H-5 and H-7; C-11 with H-5, and C-12 with H-5 and H-7) established a 1-indanone skeleton and a 2,6-dimethyl-4-carboxyl substitution pattern for this new substance. Since **1** was devoid of optical

rotation between 589 and 365 nm, it was evident that the isolated compound is a racemic mixture of the two enantiomers at the C-2 asymmetric center, which can be easily racemized through the enolic form of the 1-indanone.

Table 2.1: NMR spectroscopic data [400 (^{1}H) and 100 (^{13}C) MHz, $CDCl_3$] for compound **1**.[a]

Position	δ_C, mult.	δ_H (*J* in Hz)	HMBC[b]
1	209.1, qC	-	-
2	42.0, CH	2.72, ddq (7.9, 7.0, 3.7)	1, 3, 8, 9, 10
3	36.1, CH_2	3.77, dd (18.6, 7.9)	1, 2, 4, 8, 9, 10
		3.02, dd (18.6, 3.7)	1, 2, 4, 8, 9, 10
4	127.1, qC	-	-
5	138.0, CH	8.18, d (2.0)	4, 6, 7, 9, 11, 12
6	138.1, qC	-	-
7	129.4, CH	7.79, d (2.0)	1, 5, 6, 8, 9, 12
8	137.9, qC	-	-
9	153.1, qC	-	-
10	16.2, CH_3	1.31, d (7.0)	1, 2, 3
11	171.3, qC	8.60, br[c]	[d]
12	20.9, CH_3	2.45, s	5, 6, 7

[a]These assignments were also in agreement with the COSY and HSQC spectra. [b]HMBC correlations, optimized for 8 Hz, are from proton(s) stated to the indicated carbon. [c]Carboxylic proton. [d]Not observed (Fig. 2.9-2.14).

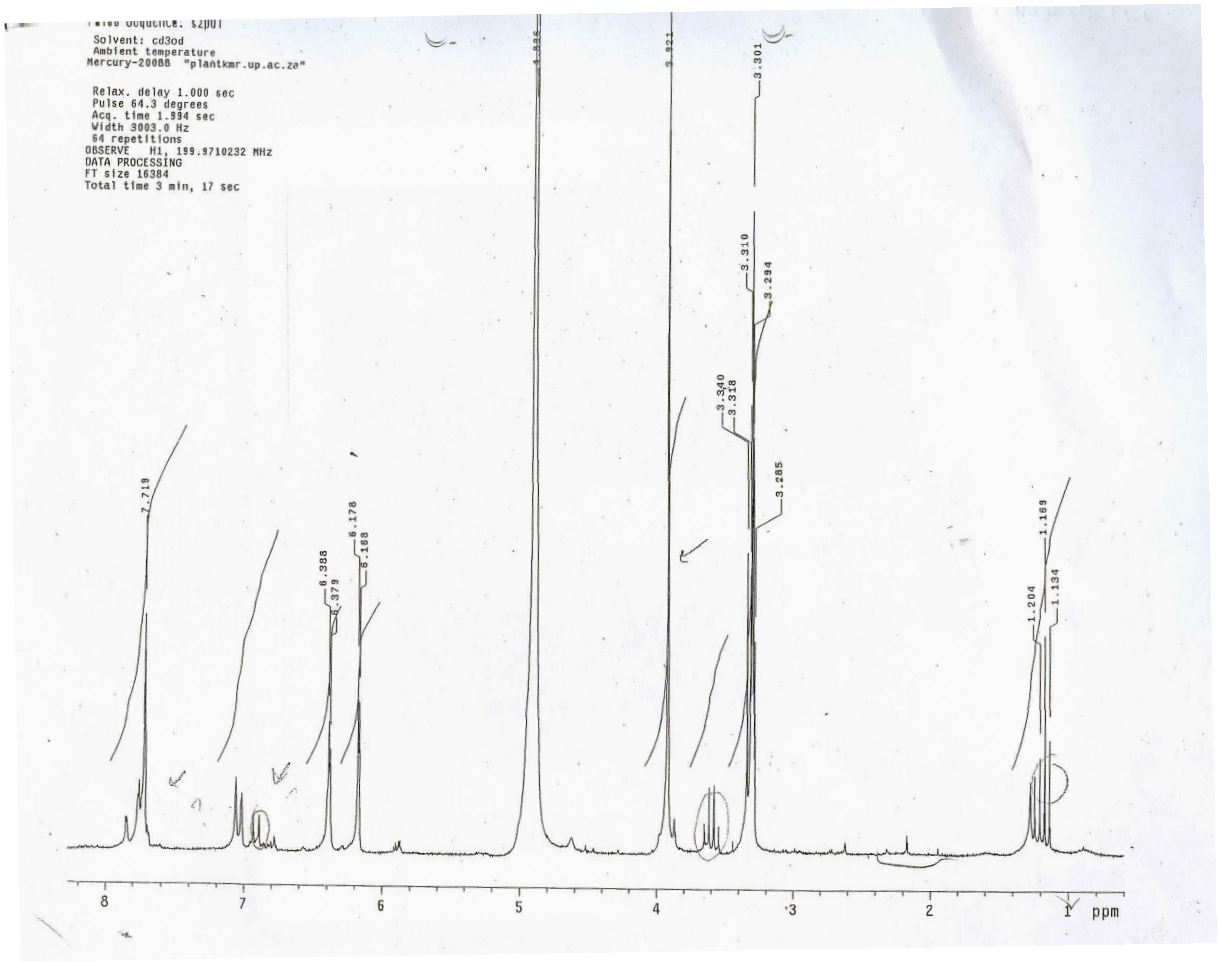

Figure 2.5: ^{1}H-NMR spectrum of tamarixetin.

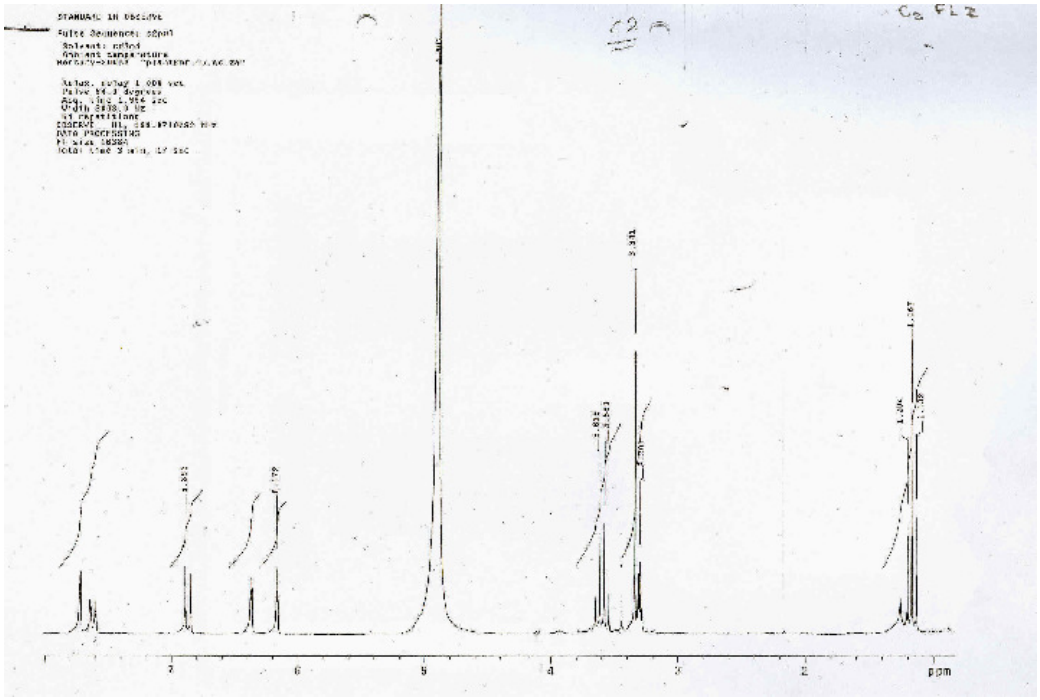

Figure 2.6: ^{1}H-NMR spectrum of quercetin.

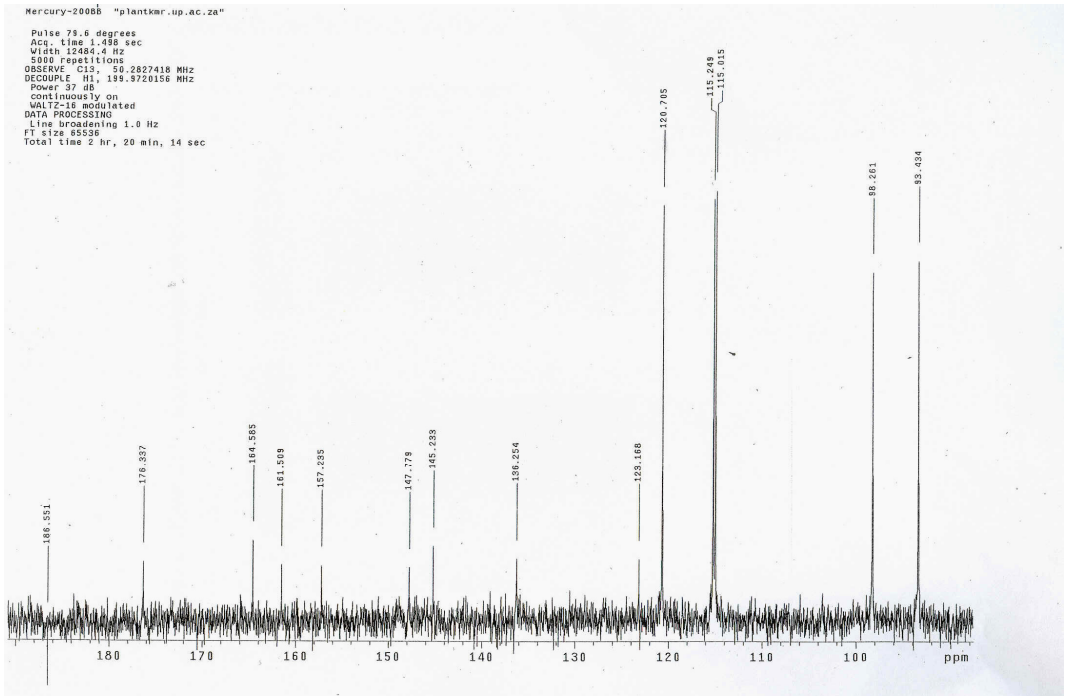

Figure 2.7: ^{13}C-NMR spectrum of quercetin.

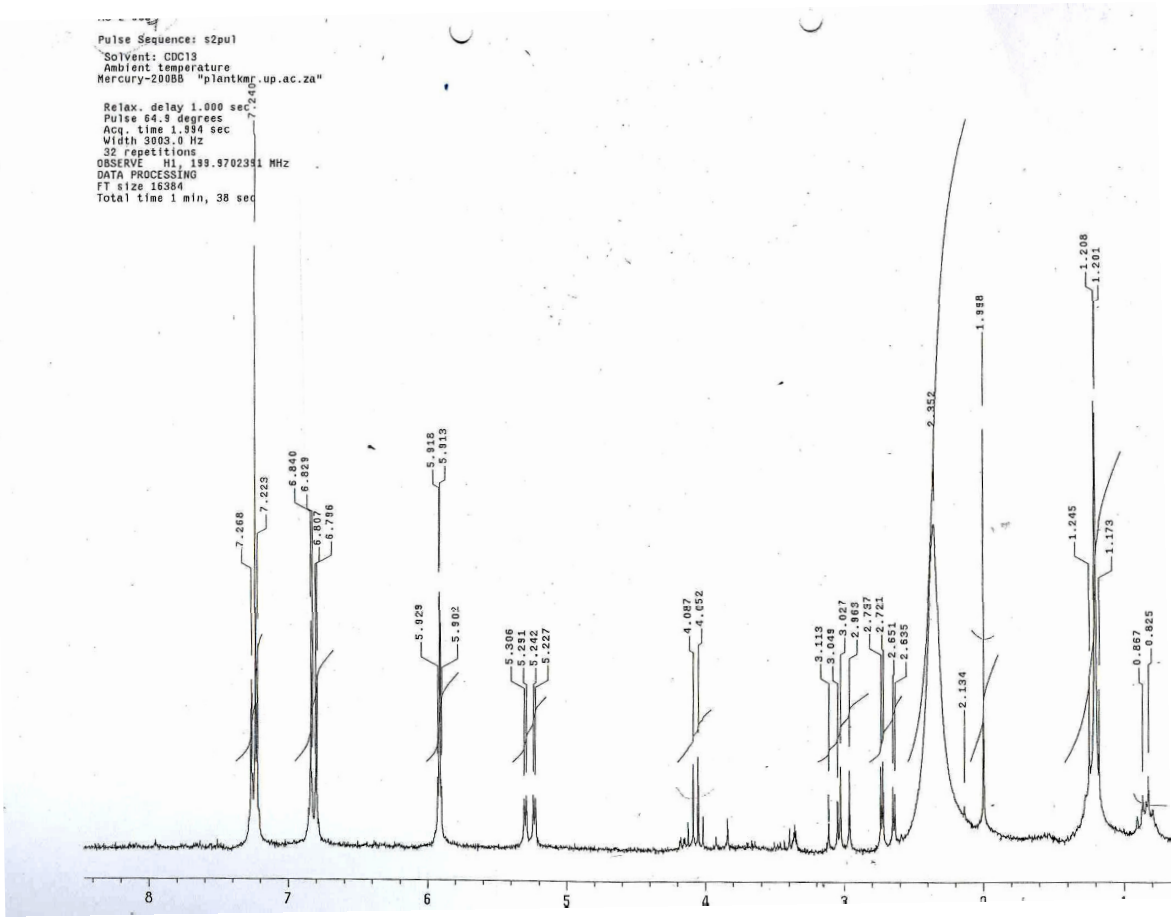

Figure 2.8: ^{1}H-NMR spectrum of eriodictyol.

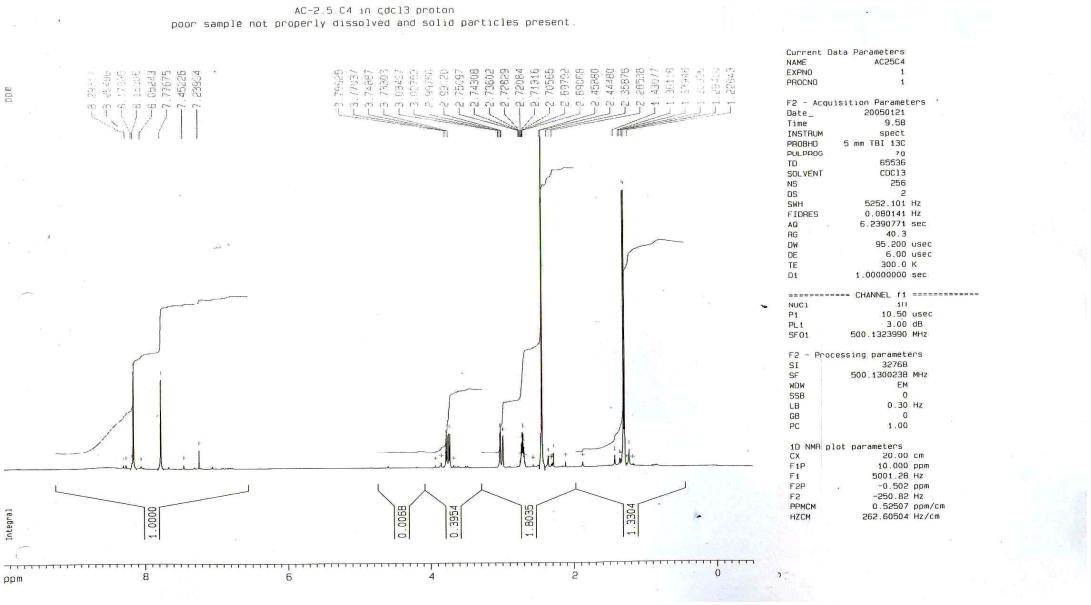

Figure 2.9: ^{1}H-NMR spectrum of indane.

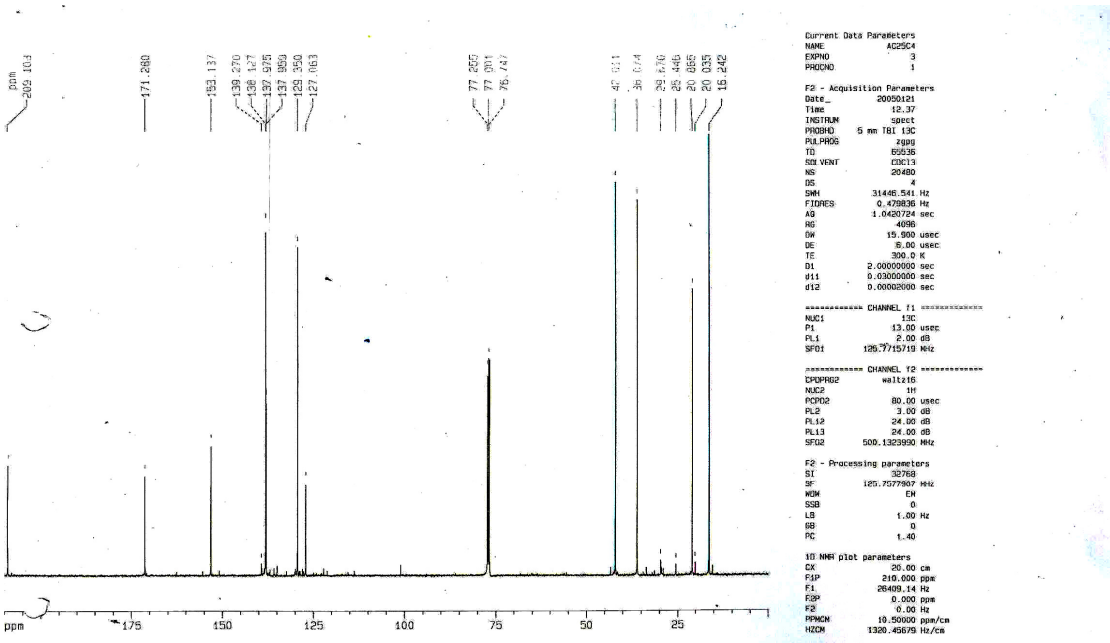

Figure 2.10: ^{13}C-NMR spectrum of indane.

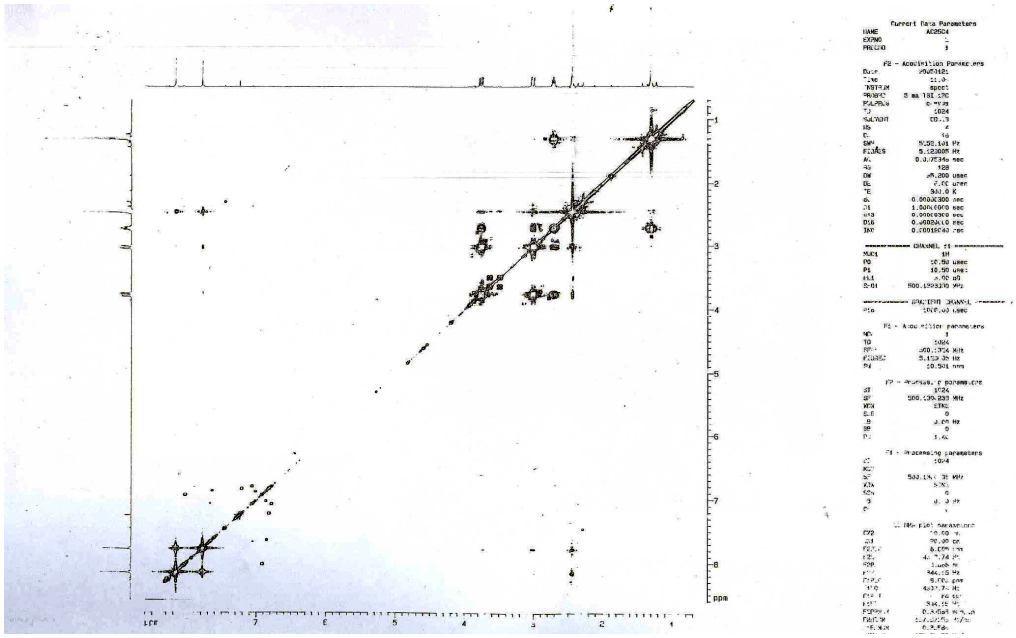

Figure 2.11: COSY spectrum of indane.

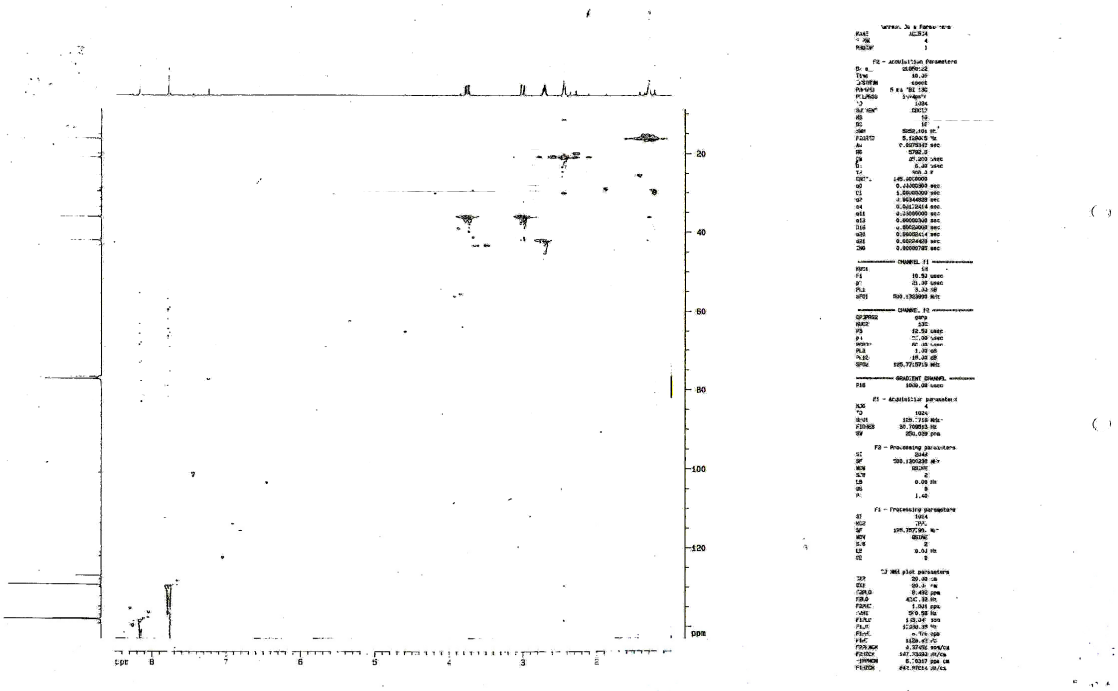

Figure 2.12: HMQC spectrum of indane.

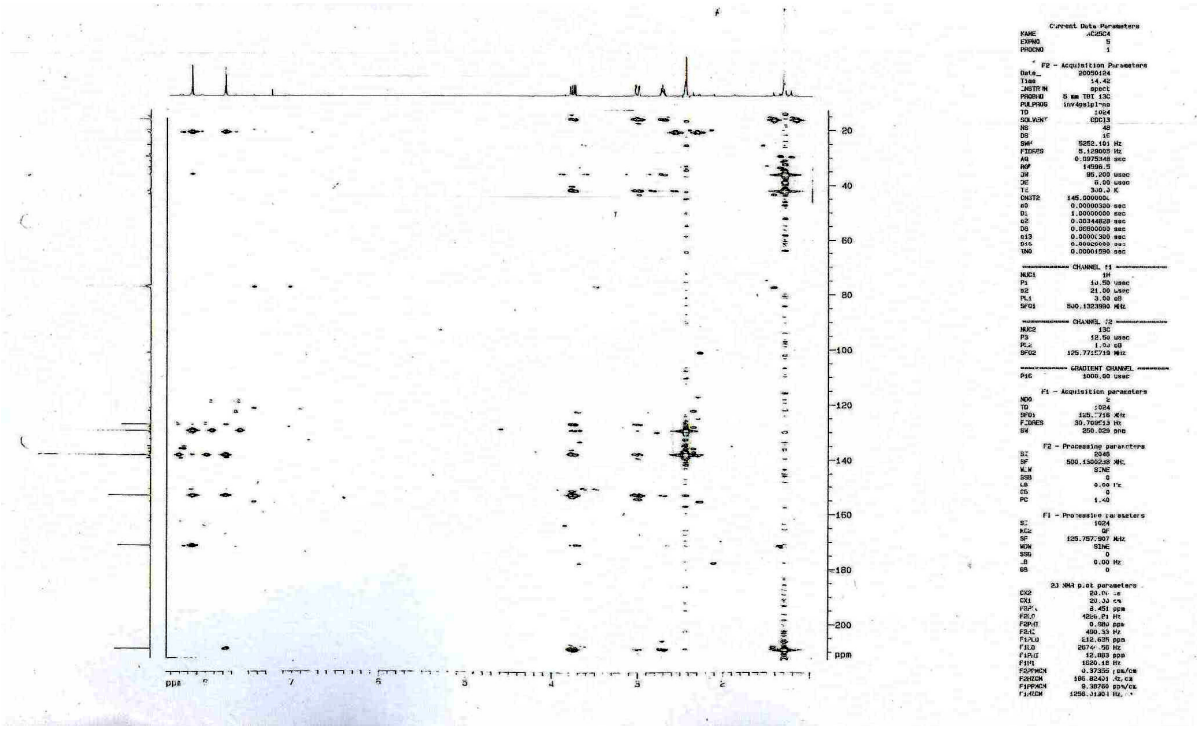

Figure 2.13: HMBC spectrum of indane.

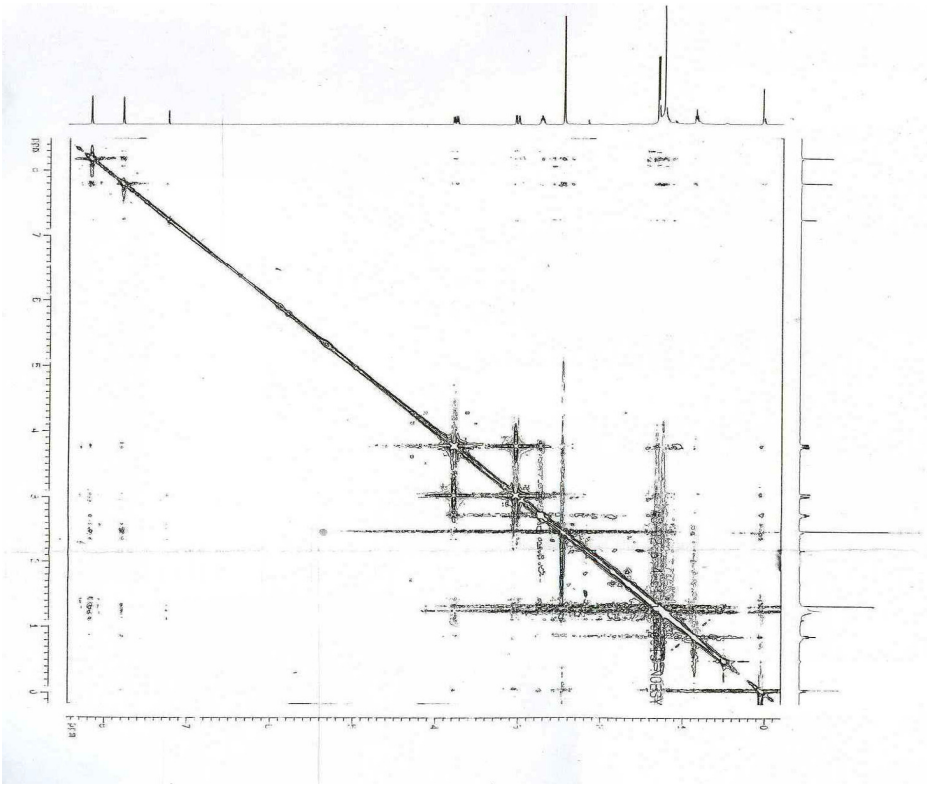

Figure 2.14: NOESY spectrum of indane.

Steenkrotin A (2): colourless needles (EtOAc-petroleum ether), mp 219-221 ºC; $[\alpha]_D^{20}$ +188.6 (*c* 0.324, $CHCl_3$); UV (MeOH) λ_{max} (log ε) 227 (3.96) 250 shoulder (3.68) nm; IR (KBr) ν_{max} 3359, 3050, 3020, 2971, 2940, 1702, 1649, 1454, 1375, 1286, 1231, 1112, 1055, 1019, 905, 743, 650 cm^{-1}; ^1H and ^{13}C NMR: see Table 2.2; EIMS *m/z* 330 $[M]^+$ (3)(Fig. 2.21), 315 (0.5), 312 (2), 297 (0.5), 262 (60), 244 (27), 227 (14), 187 (18), 177 (62), 161 (30), 160 (26), 145 (16), 121 (29), 97 (35), 91 (14), 83 (13), 77 (14), 69 (100), 55 (29); *anal.* C 72.43%, H 8.25%, calcd for $C_{20}H_{26}O_4$, C 72.70%, H 7.93%.

The ^1H and ^{13}C NMR data (Fig. 2.16 and 2.17, Table 2.2) of steenkrotin A indicated the presence of five methyl groups 1.42s (δ_c 21.7), 1.01s (δ_c 20.6), 1.06s (δ_c 16.9), 1.03, d (*J*=3.1 δ_c 16.4) and 1.05d (*J*=3.1 δ_c 14.8), two ketonic group at δ_c 205.1s, 212.7s, one olefinic proton at δ_H 6.55s (δ_c 134.3), two methylene group at δ_H 1.96dd, 2.19dd (δ_c 35.9t), 1.66ddd, 1.84dd (δ_c 29.6), protons at 4.21 d (*J*=3.7, δ_c 79.3) in addition to 0.68dd (*J*=2.3, 10.0, δ_c 25.4) characteristic of a cyclopropyl group (Table 2.2).

The HMBC cross peaks showed correlation of the methyl group at 1.05 with carbons at δ_c 205.1 and 35.9 and the ethylene protons at δ_H 1.96, 2.19 showed correlations with δ_c 62.5, 205.1, 212.7, and 143.7, and correlations between δ_H 6.55 and δ_C 205.1, 62.5; furthermore, the band at 1424 cm^{-1} in IR indicated the presence of αβ-unsaturated ketone. These data clearly confirm the existence of the partial structure (Fig. 2.15).

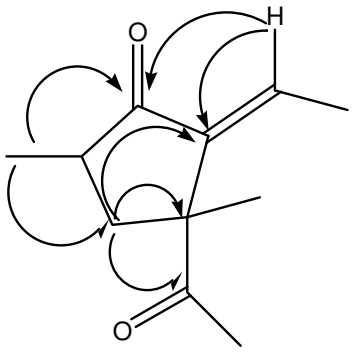

Figure 2.15: HMBC correlation of partial structure.

The other structural parts were confirmed from the other HMBC correlations as follows: the methyl group at 1.03 showed correlations with carbons at δ_c 62.5, 212.7, 29.6 in addition to the correlations δ_H 0.68/ δ_c 74.7, 39.8, 20.6, 21.7; δ_H 6.55/ δ_c 134.9, 75.1, 63.3, 21.7. All the foregoing information in addition to the other data of HMBC, DEPT 135, COSY 45, and HMQC (Fig. 2.18 and 2.20) confirm the plane structure of **2**.

The NOESY correlations of the compound (Fig. 2.19) showed correlations between methyl-20, H-8, H-6, H-5, H-11, H-3 (δ_H 2.19) with H-12 (δ_H 1.66); H-13/H-12, and finally between H-3 (δ_H 1.96)/H-2. These data indicate that the groups; methyl-20, H-8, H-6, H-5, H-11, H-3 (δ_H 2.19) and H-12 (δ_H 1.66) are on one side and the groups H-13, H-12, H-3 (δ_H 1.96) and H-2 are on the other side.

Finally the structure of steenkrotin A (**2**, $C_{20}H_{26}O_4$) was confirmed from X-ray diffraction studies. Figure 2.22 is a perspective view of the molecule of **2** showing its relative configuration. Moreover, the 1D and 2D NMR spectroscopic data of **2** (Tables 2.2 and 2.3) were in complete agreement with the proposed structure.

Table 2.2: NMR spectroscopic data [400 (^{1}H) and 100 (^{13}C) MHz, $CDCl_3$] for Compounds **2** – 4.[a]

		2			**3**			**4**	
position	δ_C,mult.	δ_H (*J* in Hz)	HMBC[b]	δ_C,mult.	δ_H (*J* in Hz)	HMBC[b]	δ_C,mult.	δ_H (*J* in Hz)	HMBC[b]
1[c]	35.9, CH_2	1.98, dd (12.5, 11.4)	2, 8, 9, 10, 19	39.5, CH_2	2.13, dd (13.1, 12.5)	2, 3, 8, 9, 10, 19	38.8, CH_2	1.72, dd (12.8, 11.3)	2, 8, 9, 10, 19
		2.20, dd (12.5, 8.4)	2, 3, 9, 10, 19		2.63, dd (13.1, 7.2)	2, 3, 4, 9, 10		2.15, dd (12.8, 8.4)	2, 3, 4, 8, 9, 10
2	39.73, CH	2.31, ddq (11.4, 8.4, 7.0)	1, 3, 4, 9, 19	39.2, CH	2.27, ddq (12.5, 7.2, 7.0)	1, 3, 9, 19	38.7, CH	2.52, ddq (11.3, 8.4, 7.0)	1, 3, 19
3	206.5 qC	-	-	206.5, qC	-	-	204.7, qC	-	-
4	143.7, qC	-	-	144.6, qC	-	-	142.7, qC	-	-
5	134.5, CH	6.50, s	3, 6, 7, 9, 20	129.7, CH	6.36, d (0.8)	3, 6, 7, 9, 20	130.4, CH	6.69, d (1.0)	3, 6, 7, 9, 20
6	75.1, qC	-	-	68.6, qC	-	-	74.9, qC	-	-
7	79.2, CH	4.22, d (3.9)	5, 6, 8, 9, 20	75.6, CH	4.30, dd (2.5, 0.8)	5, 6, 8, 9, 20	71.4, CH	5.60, dd (2.3, 1.0)	5, 6, 8, 9, 14, 20
8	40.8, CH	2.69, d (3.9)	1, 4, 6, 7, 9, 10, 13, 15	36.5, CH	3.05, d (2.5)	1, 9, 10, 13, 14	44.6, CH	4.44, dd (2.3, 0.8)	1, 9, 10, 13, 14
9	62.6, qC	-	-	55.6, qC	-	-	52.8, qC	-	-
10	213.1, qC	-	-	212.4, qC	-	-	211.3, qC	-	-
11	39.73, CH	2.95, ddq (12.5, 6.8, 6.4)	10, 12, 18	44.5, CH	3.08, ddq (7.4, 7.1, 3.4)	9, 10, 12, 13, 18	43.1, CH	3.79, ddq (10.7, 2.4, 6.7)	10, 12, 13, 18
12[c]	29.6, CH_2	1.67, ddd (14.3, 6.8, 2.4)	10, 11, 13, 14, 15, 18	29.4, CH_2	1.93, ddd (15.7, 8.9, 3.4)	10, 11, 13, 14, 15, 18	29.3, CH_2	2.22, ddd (16.3, 4.5, 2.4)	10, 11, 13, 14, 15, 18
		1.83, ddd (14.3, 12.5, 10.1)	11, 13, 15, 18		1.79, ddd (15.7, 7.1, 4.9)	10, 11, 13, 14, 15, 18		2.07, ddd (16.3, 6.7, 4.5)	10, 11, 13, 14, 15, 18
13	25.3, CH	0.68, dd (10.1, 2.4)	11, 12, 14, 15, 16, 17	60.3, CH	2.93, dd (8.9, 4.9)	11, 12, 14, 15, 16, 17	61.2, CH	2.66, td (4.5, 0.8)	8, 11, 12, 14, 15, 16, 17
14	74.1, qC	-	-	110.1, qC	-	-	208.2, qC	-	-
15	22.8, qC	-	-	87.6, qC	-	-	87.4, qC	-	-
16	20.7, CH_3	1.03, s	13, 14, 15, 17	22.3, CH_3[d]	1.45, s[d]	13, 15, 17	24.4, CH_3[d]	1.48, s[d]	13, 15, 17
17	16.5, CH_3	1.07, s	13, 14, 15, 16	25.74, CH_3[d]	1.34, s[d]	13, 15, 16	24.7, CH_3[d]	1.44, s[d]	13, 15, 16
18	17.0, CH_3	1.06, d (6.4)	10, 11, 12	18.0, CH_3	1.27, d (7.4)	10, 11, 12	18.3, CH_3	1.20, d (6.7)	10, 11, 12
19	14.9, CH_3	1.04, d (7.0)	1, 2, 3	14.7, CH_3	1.07, d (7.0)	1, 2, 3	15.6, CH_3	1.06, d (7.0)	1, 2, 3
20	21.8, CH_3	1.43, s	5, 6, 7	25.70, CH_3	1.47, s	5, 6, 7	20.9, CH_3	1.52, s	5, 6, 7
6β-OOAc	-	-	-	-	[e]	-	167.0, qC 17.3, CH_3	2.08, s	[f]
7α-OAc	-	-	-	-	[e]	-	169.9, qC 21.1, CH_3	2.05, s	[f]
15-OAc	-	-	-	-	[e]	-	168.5, qC 21.0, CH_3	1.87, s	[f]

[a]All these assignments were in agreement with COSY and HSQC spectra, and with 1D NOESY experiments. [b]HMBC correlations, optimized for 8 Hz, are from proton(s) stated to the indicated carbon. [c]For methylene groups, the first reported δ value belongs to the α-proton and the second δ value is assigned to the β-proton. [d]Interchangeable assignments. [e]Hydroxyl protons at δ 5.89 br s, 3.56 br, and 2.16 s. [f]HMBC correlations for the OAc groups: δ 167.0, 169.9, and 168.5 with the *Me*COO group at δ 2.08, 2.05, and 1.87, respectively, and δ 169.9 also with H-7.

Table 2.3: Significant NOE Data for Compounds **2** – **4**.

Compound	Irradiated proton (s) (δ)	Observed NOEs
2	H-1α (1.98)	H-1β,[a] H-8α,[b] Me-19[b]
	H-5 (6.50)	Me-20[b]
	H-7β (4.22)	H-8α,[b] Me-16 + Me-17,[c] Me-20[b]
	H-8α (2.69)	H-1α,[c] H-1β,[c] H-7β,[b] H-11α,[a], Me-17[b]
	H-11α (2.95)	H-1β,[b] H-8α,[a] H-12α,[b] H-12β,[c] Me-18[a]
	H-13β (0.68)	H-12α,[c] H-12β,[a] Me-16[b]
	Me-20 (1.43)	H-5,[c] H-7β,[b] Me-16[c]
3	H-1β (2.63)	H-1α,[a] H-2β,[a] Me-18[b]
	H-5 (6.36)	Me-20[b]
	H-7β (4.30)	H-8α,[b] Me-20[b]
	H-13β (2.93)	H-12α,[c] H-12β,[b] Me-18[c]
	Me-18 (1.27)	H-1β,[c] H-11α,[c] H-13β,[c] H-12α + H-12β[c]
	Me-19 (1.07)	H-1α,[b] H-1β,[c], H-2β[b]
4	H-1α (1.72)	H-1β,[a] H-2β,[b] Me-19[b]
	H-2β (2.52)	H-1α,[c] H-1β,[b] Me-19[b]
	H-5 (6.69)	Me-20[a]
	H-7β (5.60)	H-8α,[a] Me-20[a]
	H-8α (4.44)	H-5,[c] H-7β,[a] H-11α,[a] H-12α,[b] Me-16 + Me-17,[b] 15-OAc[c]
	H-11α (3.79)	H-8α,[a] H-12α,[b] H-12β,[c] Me-18,[b] 15-OAc[c]
	H-13β (2.66)	H-12α + H-12β,[a] Me-16 + Me-17,[a] Me-18[b]
	Me-18 (1.20)	H-11α,[c] H-13β,[c] H-12α + H-12β[b]
	Me-19 (1.06)	H-1α,[b] H-1β,[c] H-2β,[b] 7α-OAc[c]

[a]Strong NOE enhancement (>4%). [b]Medium NOE enhancement (1.5 - 4%). [c]Weak NOE enhancement (0.5 – 1.5%).

X-Ray Structure Determination of 2. The crystallographic data set was collected at 20 °C on a Siemens P4 diffractometer fitted with a Bruker 1K CCD detector and SMART control software using graphite-monochromated, Mo-Kα radiation by means of a combination of phi and omega scans. Data reduction was performed using SAINT+ and the intensities were corrected for absorption using SADABS. The structures were solved by direct methods using SHELXTS and refined by full-matrix least squares using SHELXTL and SHELXL-97. All hydrogen atoms for the structure of **2** were located experimentally. In the refinement, the hydrogen atoms were refined without any positional constrains. Isotropic displacement parameters for the non-methyl hydrogen atoms were calculated as 1.2 × U_{eq} of the atom to which they were attached, and the corresponding value for methyl hydrogen atoms was 1.5 × U_{eq} of the carbon atom to which they were attached. All non-hydrogen atoms were refined with anisotropic displacement parameters. Drawings of the structure (Fig. 2.22) were produced using Ortep-3 for Windows (Farruggia, 1997), Mercury and POV-Ray for Windows.

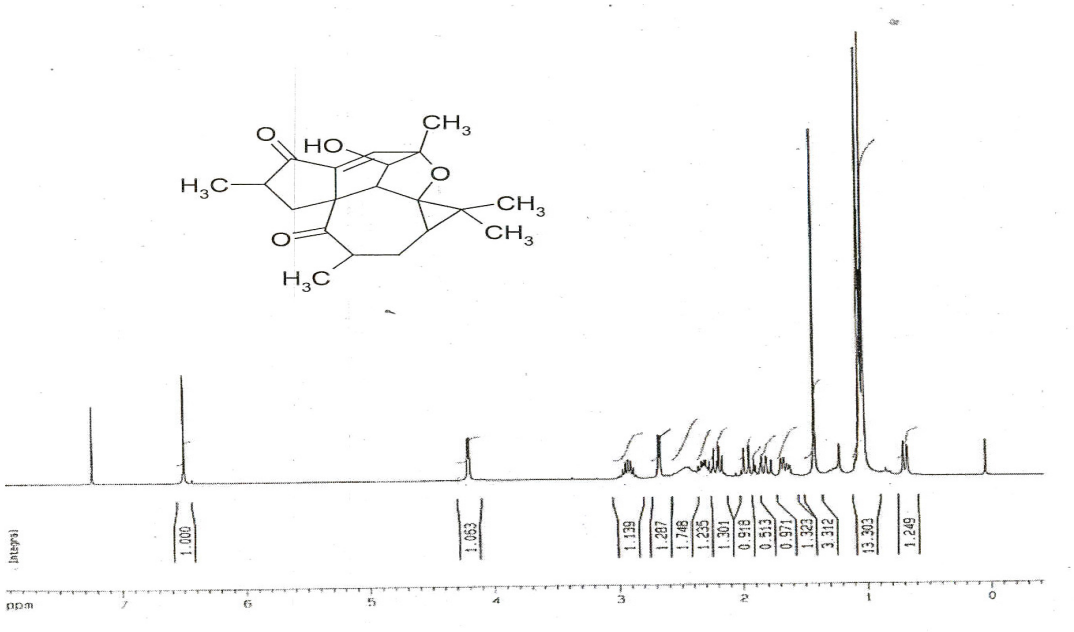

Figure 2.16: [1]H-NMR spectrum of steenkrotin A.

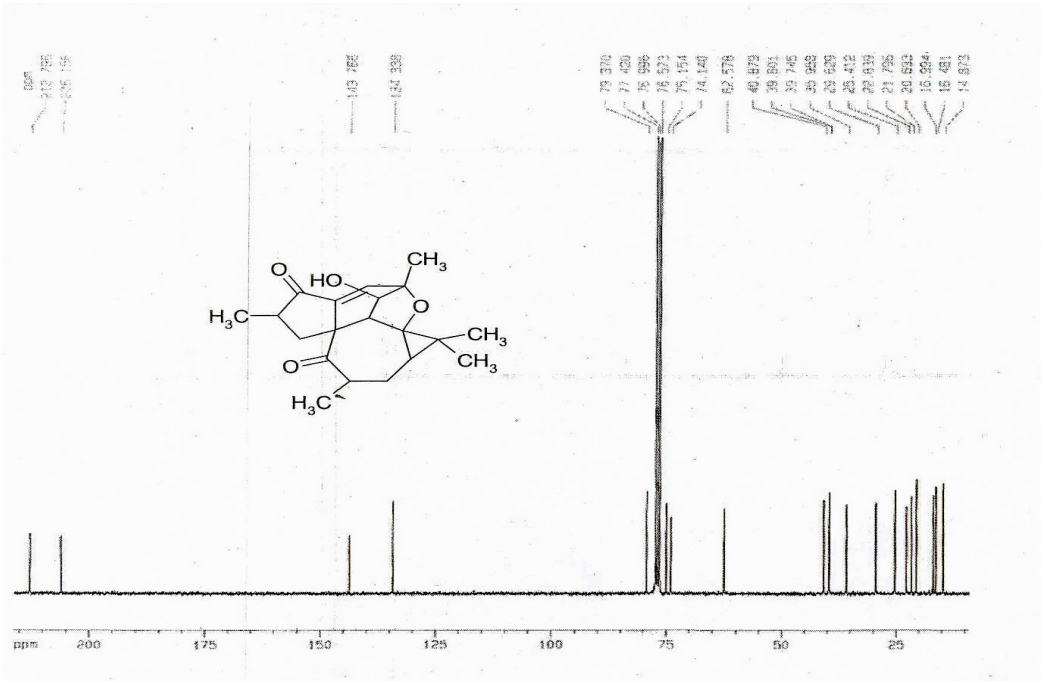

Figure 2.17: ^{13}C-NMR spectrum of steenkrotin A.

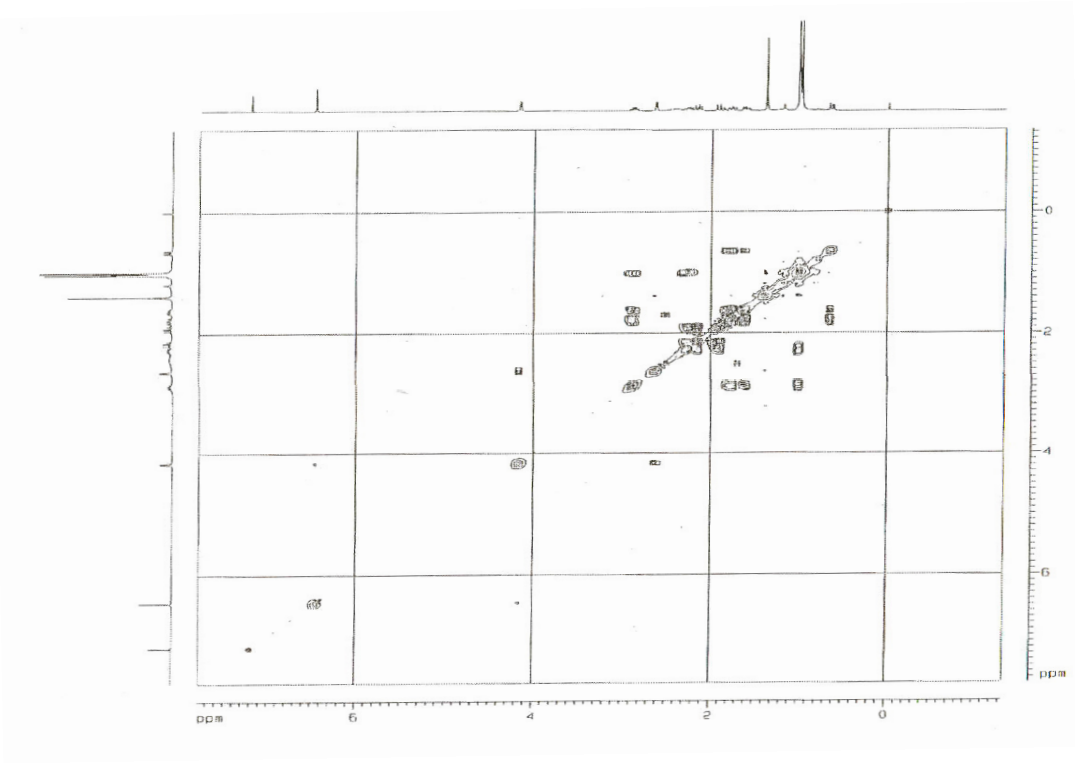

Figure 2.18: COSY spectrum of steenkrotin A.

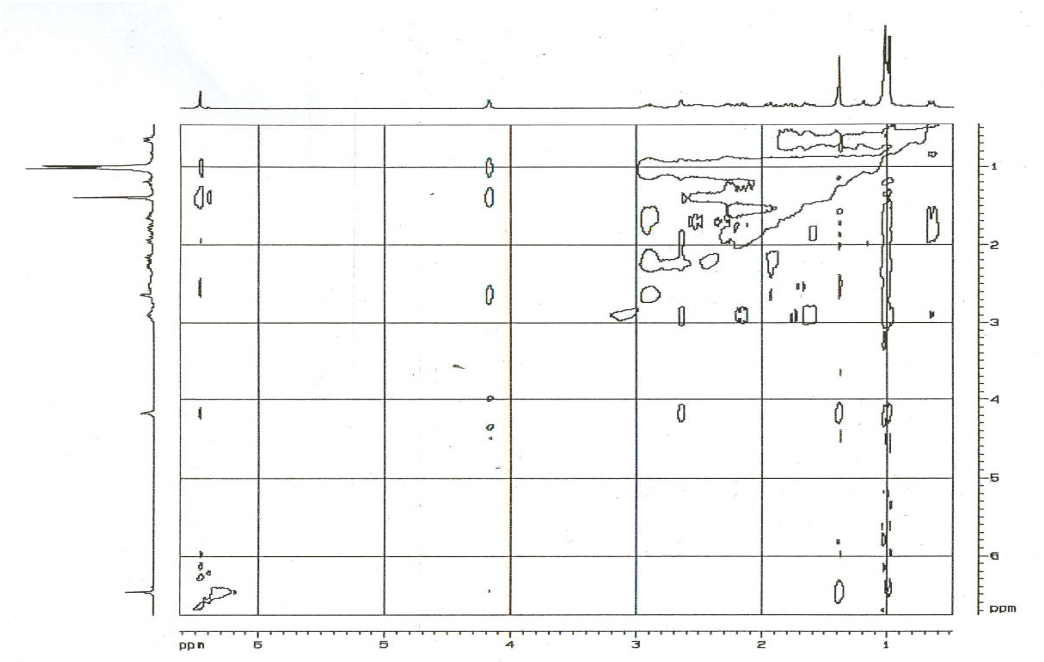

Figure 2.19: NEOSY spectrum of steenkrotin A.

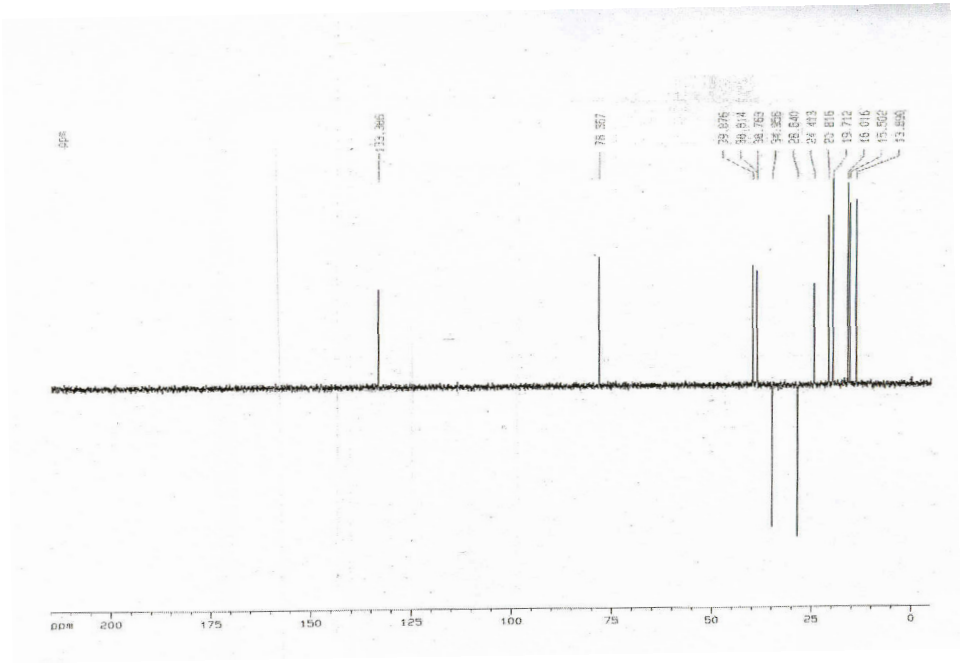

Figure 2.20: Dept 135 spectrum of steenkrotin A.

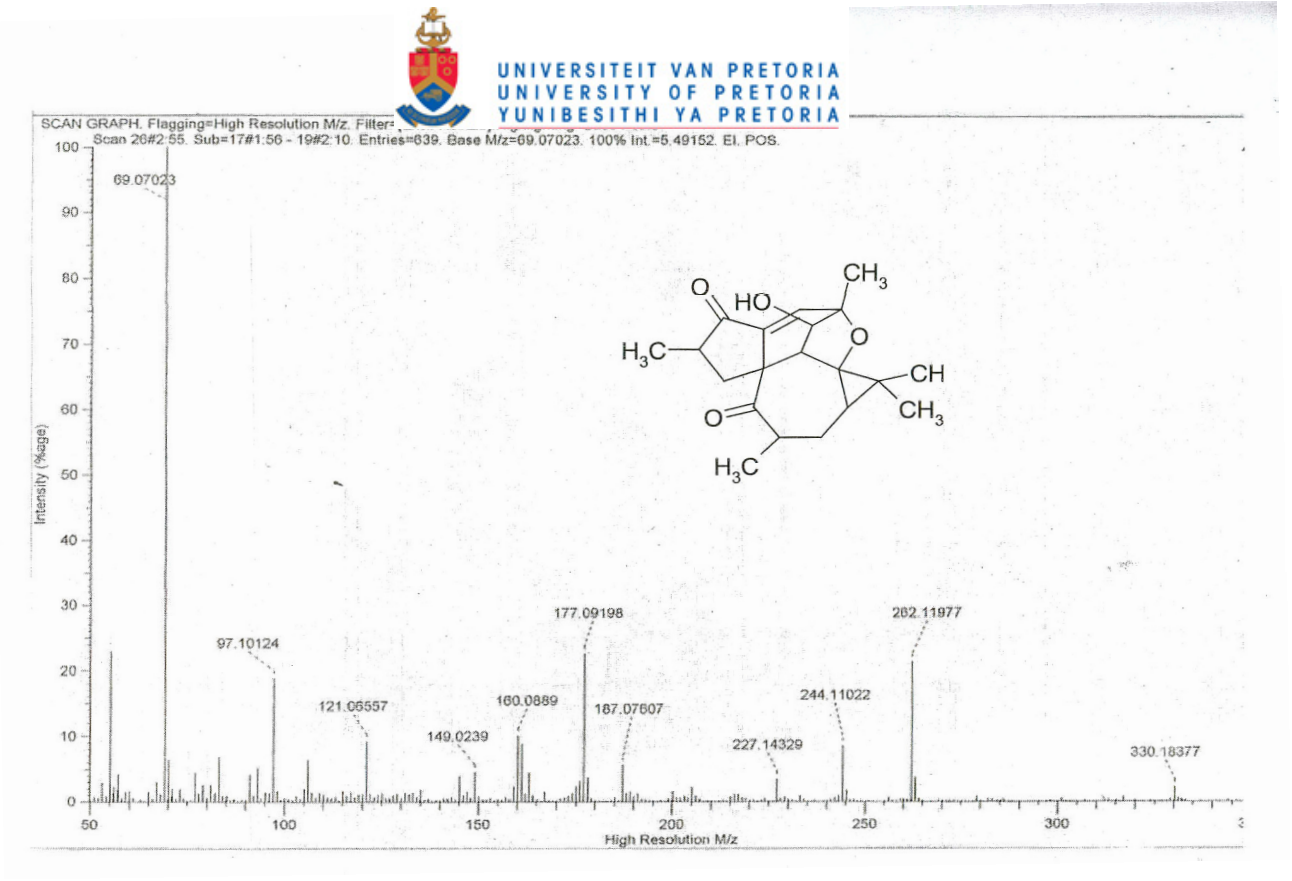

Figure 2.21: MS data of steenkrotin A.

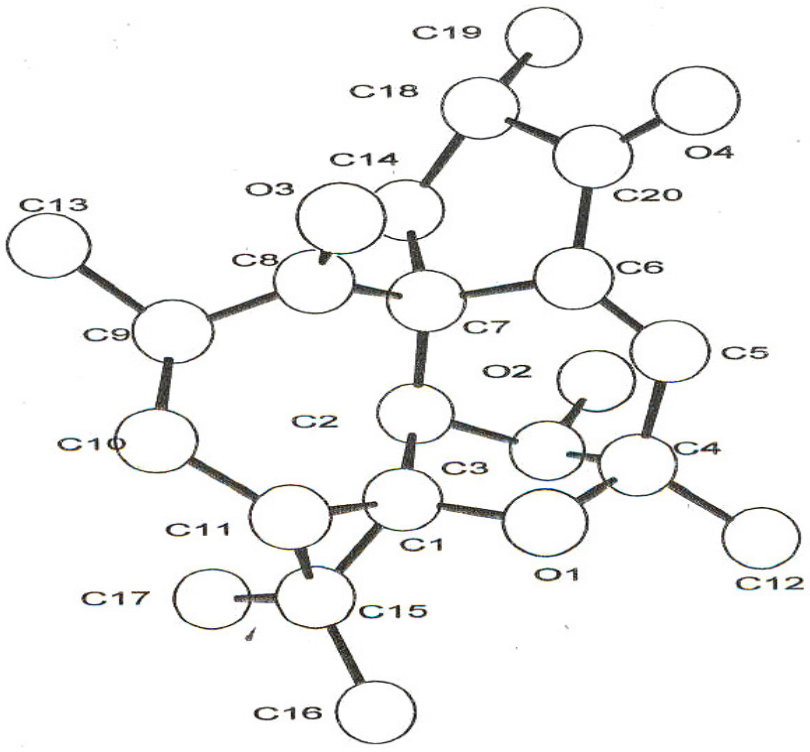

Figure 2.22: X-ray structure of steenkrotin A.

Steenkrotin B (3): colourless fine needles (MeOH), mp 130-132 ºC (decomp.); $[\alpha]_D^{20}$ +24.4 (*c* 0.119, $CHCl_3$); UV (MeOH) λ_{max} (log ε) 233 (3.98) nm; IR (KBr) ν_{max} 3435, 2976, 2932, 1731, 1691, 1676, 1457, 1372, 1194, 1078, 901 cm^{-1}; ^1H and ^{13}C NMR: see Table 2.2; (ESI)MS positive mode *m/z* 403 $[M+Na]^+$, 783 $[2M+Na]^+$; (ESI)MS negative mode *m/z* 379 $[M-H]^-$; EIMS *m/z* 380 $[M]^+$ (0.3), 362 (1), 348 (1), 338 (25), 305 (19), 264 (27), 245 (21), 219 (27), 203 (38), 187 (45), 177 (56), 161 (55), 152 (39), 141 (43), 121 (40), 95 (31), 91 (41), 85 (41), 83 (45), 71 (57), 69 (54), 55 (100); *anal.* C 63.31%, H 7.36%, calcd for $C_{20}H_{28}O_7$, C 63.14%, H 7.42%. Steenkrotin B (**3**, $C_{20}H_{28}O_7$) showed ^1H, ^{13}C, COSY, HSQC, and HMBC NMR spectra (Fig. 2.23-2.28) very similar to those of **2** (Table 2.2). The observed differences were consistent with the presence in **3** of a hydroxyisopropyl group [δ_H 1.45 and 1.34 (Me-16 and Me-17); δ_C 22.3 and 25.7 (C-16 and C-17), and 87.6, qC, C-15] [δ_H 1.45 and 1.34 (Me-16 and Me-17); δ_C 22.3 and 25.7 (C-16 and C-17), and 87.6, qC, C-15] and a hemiacetal carbon (δ 110.1, qC, C-14) instead of the pentasubstituted cyclopropane of **2**. This structural difference was also supported by the HMBC spectra, because **2** showed correlations through three bonds between C-15 and H-8, and between C-14 and Me-16 and Me-17, that were not observed for **3** (Table 2.2). Three of the seven oxygen atoms of **3** were involved in two ketones [δ 206.5 (C-3) and 212.4 (C-10)] and in a secondary hydroxyl group [δ_H 4.30; δ_C 75.6, CH (C-7)] like in **2**, and two other oxygens must be placed at C-14 and C-15 as one of the hemiacetal oxygens and as a tertiary hydroxyl group, respectively (see above). The remaining two oxygens of **3** must be part of an endoperoxide moiety between C-6 (δ 68.6, qC) and the hemiacetalic C-14 carbon. The presence of this endoperoxide was also in agreement with molecular formula requirements (7 unsaturations) and with the observed loss of O_2 (ion at *m/z* 348) from the molecular ion (*m/z* 380) in the EI mass spectrum of **3** (Perales, 1983).

Treatment of **3** with acetic anhydride-pyridine yielded the triacetyl derivative **4** ($C_{26}H_{34}O_{10}$), the IR spectrum of which was devoid of hydroxyl absorptions. In the ^{13}C NMR spectrum of **4**, the methyl carbon of one of the acetates (δ_C 167.0, qC and 17.3, CH_3; δ_H 2.08) appeared unusually shifted ((δ_C 17.3) indicating the presence of a peroxyacetate function (Olah *et al.,*1976; Baj and Chrobok*,* 2000), which is also in agreement with molecular formula requirements. Thus, apart from the esterification of the hydroxyl groups at C-7 and C-15, the acetylation of **3** caused the hydrolysis of the 14-hemiacetal and subsequent acetylation of the resulting 6-hydroperoxide, as was

also evidenced by the appearance of an additional ketone at C-14 ((δ_C 208.2, HMBC correlated with H-7, H-8, H_2-12, and H-13, Table 2.2) in the ^{13}C NMR spectrum of **4**.

The relative stereochemistry of **3** and **4** must be identical to that of **2** for the following reasons: NOE experiments (Table 2.3) established that H-8 and H-11 are in a *cis* spatial relationship in **2** and **4**, because a strong NOE enhancement was observed in H-11 when H-8 was irradiated and vice versa. Consequently, Me-18 must be *trans* (β-oriented) with respect to H-8. Moreover, the NOE observed between H-13 and Me-18 in the 1D NOESY spectra of **2** – **4** was in agreement with a β-orientation of H-13. In the case of **2**, a *cis* arrangement between H-8α and the 1-methylene protons was supported by weak NOE enhancements, but no NOEs between these protons were observed for **3** and **4**. However, the similar ^{1}H NMR chemical shifts and the almost identical coupling constant values for H_2-1, H-2, and Me-19 in **2** – **4** (Table 2.2), together with the absence of NOE between Me-18 and Me-19, support an α-orientation for the 1-methylene and Me-19 groups in **3** and **4**, as it was established for **2** by an X-ray analysis. In addition, one of the H_2-1 protons of **3** (δ2.63) showed NOE with the close Me-18 group, and this proton must be the β-oriented one, which in turn displayed a strong NOE with H-2 and no NOE with Me-19, thus establishing an α-orientation for Me-19. This conclusion was also supported by the 1D NOESY behavior of **4**, that showed a weak NOE in H-2 (+1%) and a medium NOE in Me-19 (+3.4%) when H-1α (δ 1.72) was irradiated. For structural requirements, the α-orientation of H-8 in **2** forces to a 6β,14β closure of its cyclic ether, and **3** must also have the same stereochemistry for its endoperoxide, because steenkrotin B (**3**) also has its H-8 proton α-oriented (see above). Consequently, the 6-peroxyacetate of **4** must be β-oriented.

The cyclohexene ring of **3** and **4** adopts an envelope conformation with the flap at C-7, like in **2** (Fig. 2.4), and H-7β and 7α-OH (or 7α-OAc in **4**) are equatorial and axial substituents, respectively, thus explaining the similar $J_{7\beta,8\alpha}$values (Table 2.2) and the NOE behaviour of these compounds (Table 2.3). NOE experiments also allowed the assignment of the Me-16 and Me-17 groups in **2**, as it is shown in the formula and Table 2.2. Irradiation at δ 1.43 (Me-20) caused NOE enhancement only in one of the two C-15 methyls (δ 1.03, Me-16), whereas the signal of the other one (δ 1.07, Me-17) was enhanced when H-8α was irradiated. The assignment of the configuration for both

12-methylene protons in **2** – **4** (Table 2.2) was also supported by NOE results (Table 2.3).

To the best of our knowledge, diterpenoids **2** and **3** possess new carbon skeleta that may be derived from the tigliane (**5**) and daphnane (**6**) types, respectively, by an 8(9→10) *abeo* rearrangement. It is of interest that diterpenes belonging to **5** and **6** carbon frameworks have repeatedly been found in several *Croton* species and in other Euphorbiaceae genera (Connolly and Hill, 1991).

Transformation of Steenkrotin B (3) into Compound 4. Treatment of **3** (15.0 mg) with Ac_2O-pyridine (1:1, 4.0 ml) for 24 h at room temperature, followed with evaporation of the volatiles at 50 ºC under reduced pressure, yielded a residue which was chromatographed on a silica gel column using 10% ethyl acetate in hexane to give **4** (8 mg, 53.0 % yield): amorphous white solid; $[\alpha]_D$ (Farruggia, 1997) –99.3 (*c* 0.293, $CHCl_3$); IR (KBr) ν_{max} 2929, 1745, 1736, 1706, 1694, 1457, 1369, 1225, 1102, 1076, 1039, 945, 922, 849 cm^{-1}; ^1H and ^{13}C NMR: see Table 2.2; (ESI) MS positive mode *m/z* 529 $[M+Na]^+$, 1035 $[2M+Na]^+$; *anal.* C 61.83%, H 6.80%, calcd for $C_{26}H_{34}O_{10}$, C 61.65%, H 6.77% (Fig. 2.29-2.34).

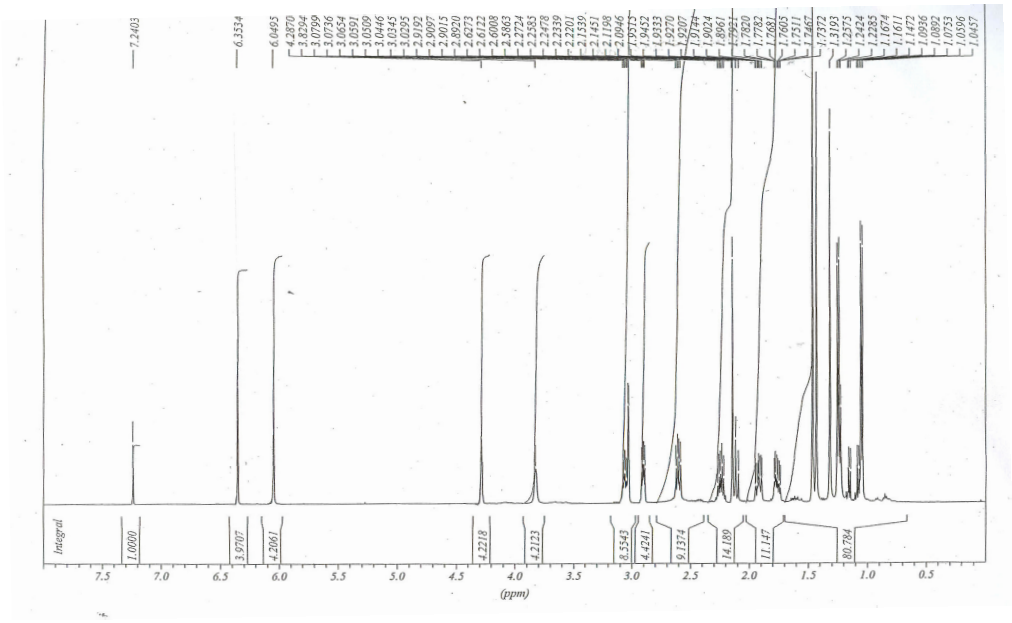

Figure 2.23: ^1H-NMR spectrum of steenkrotin B.

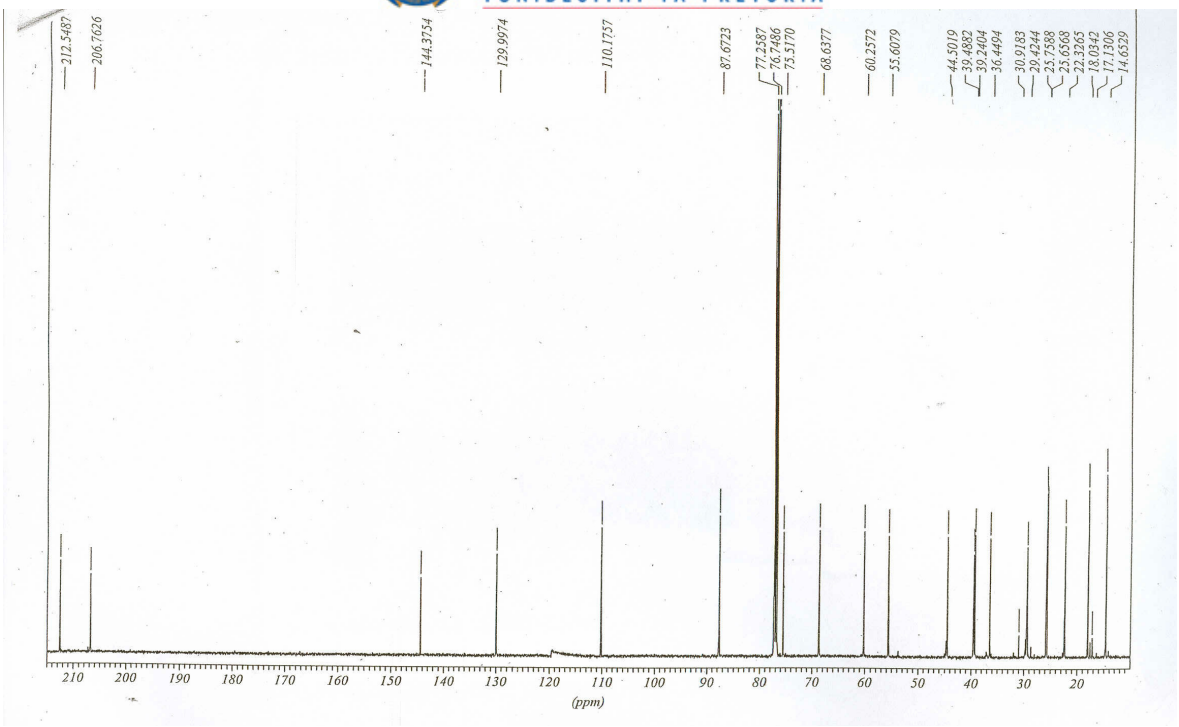

Figure 2.24: ^{13}C-NMR spectrum of steenkrotin B.

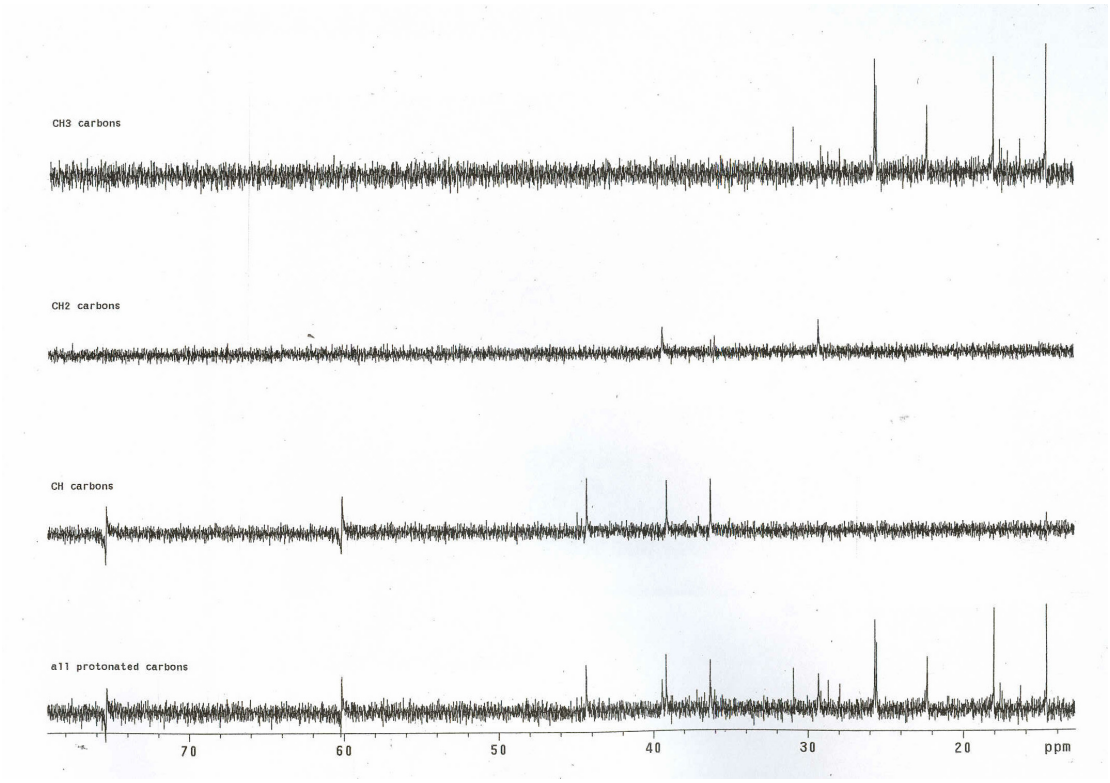

Figure 2.25: Dept spectrum of steenkrotin B.

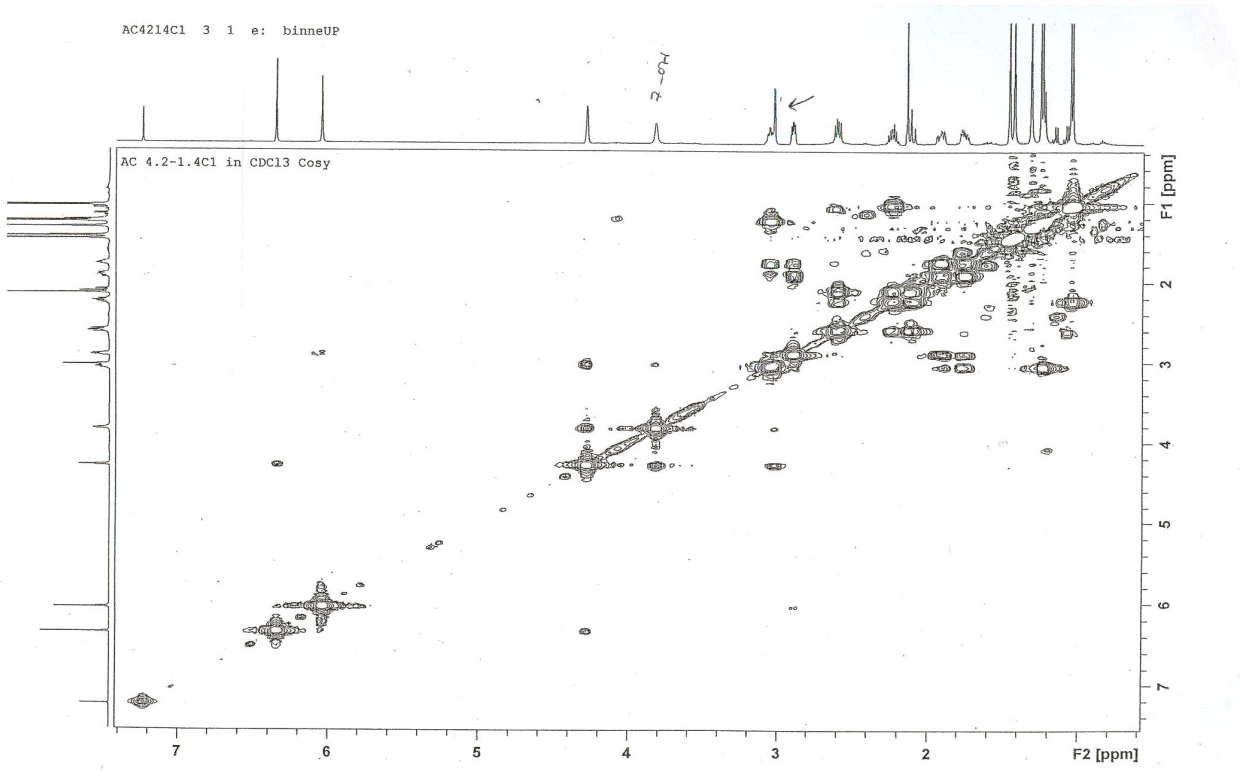

Figure 2.26: COSY spectrum of steenkrotin B.

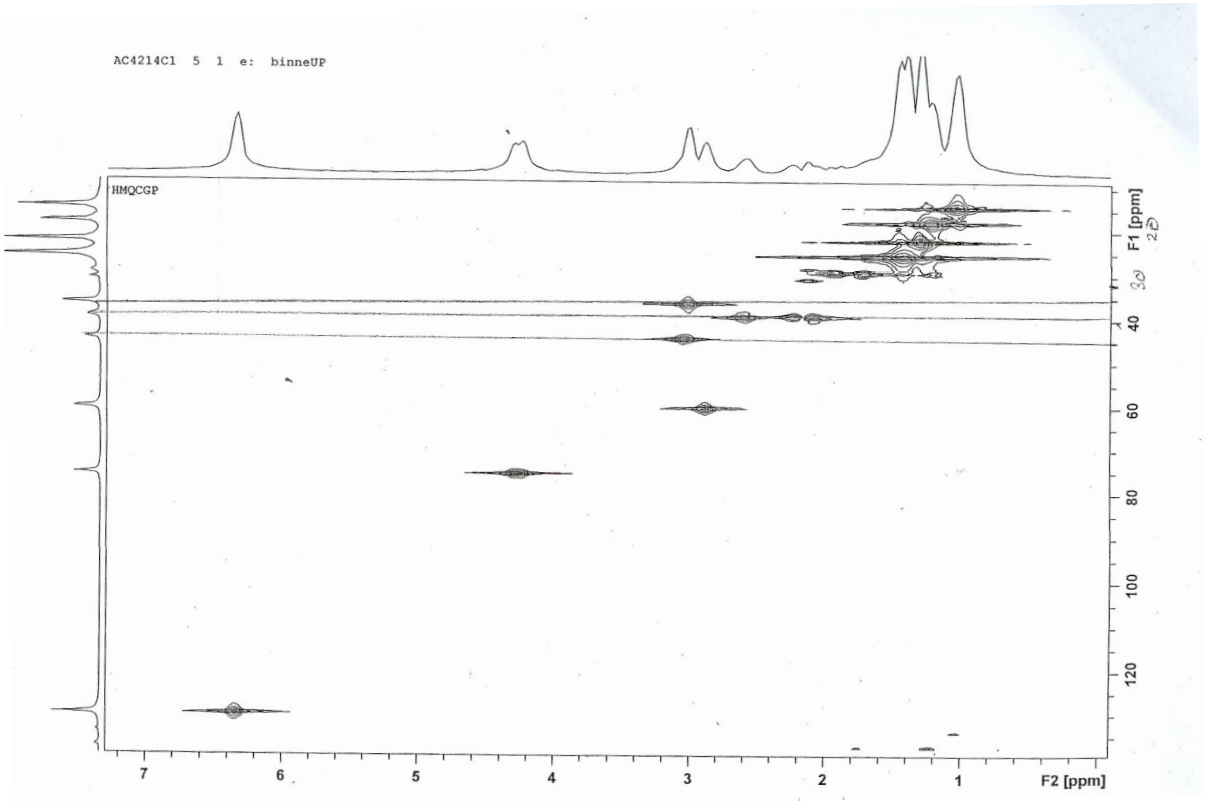

Figure 2.27: HMQC spectrum of steenkrotin B.

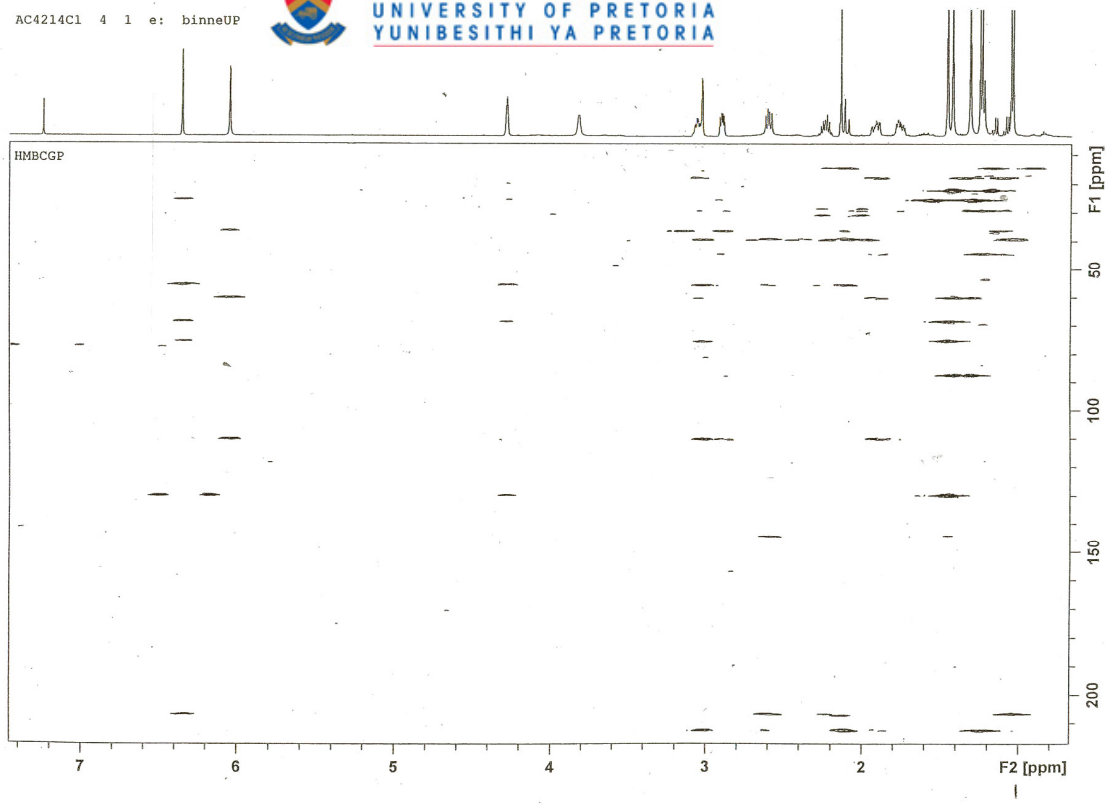

Figure 2.28: HMBC spectrum of steenkrotin B.

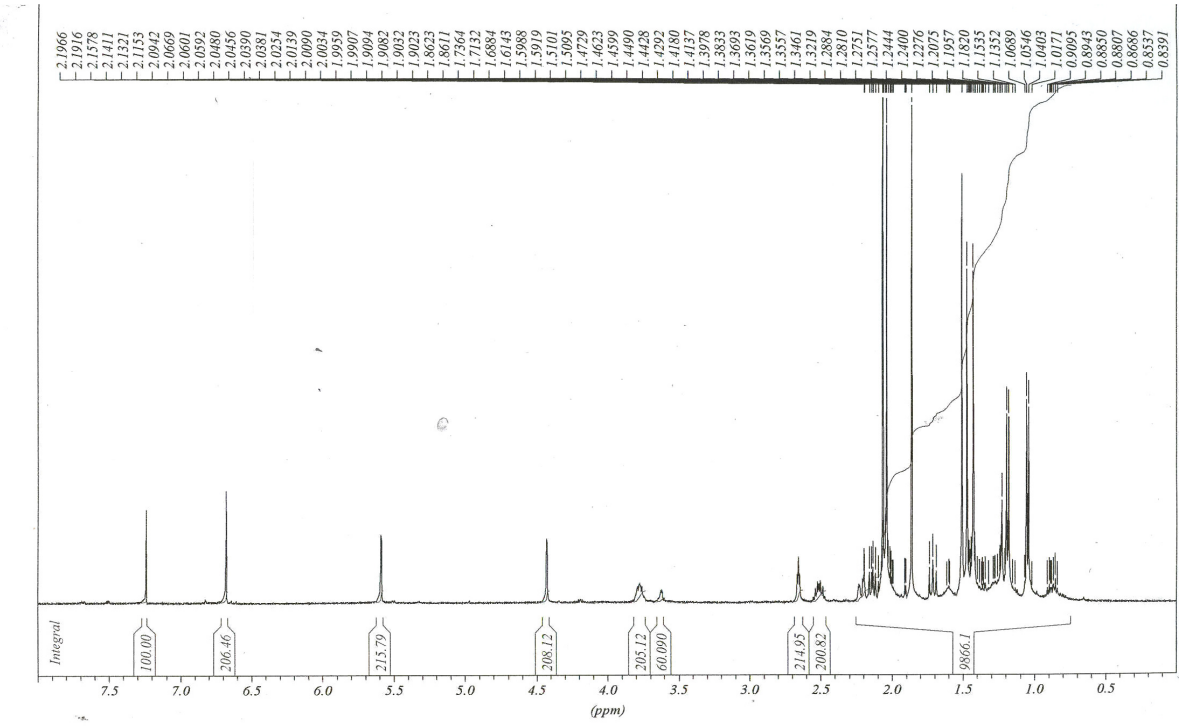

Figure 2.29: ^{1}H-NMR spectrum of steenkrotin B acetate.

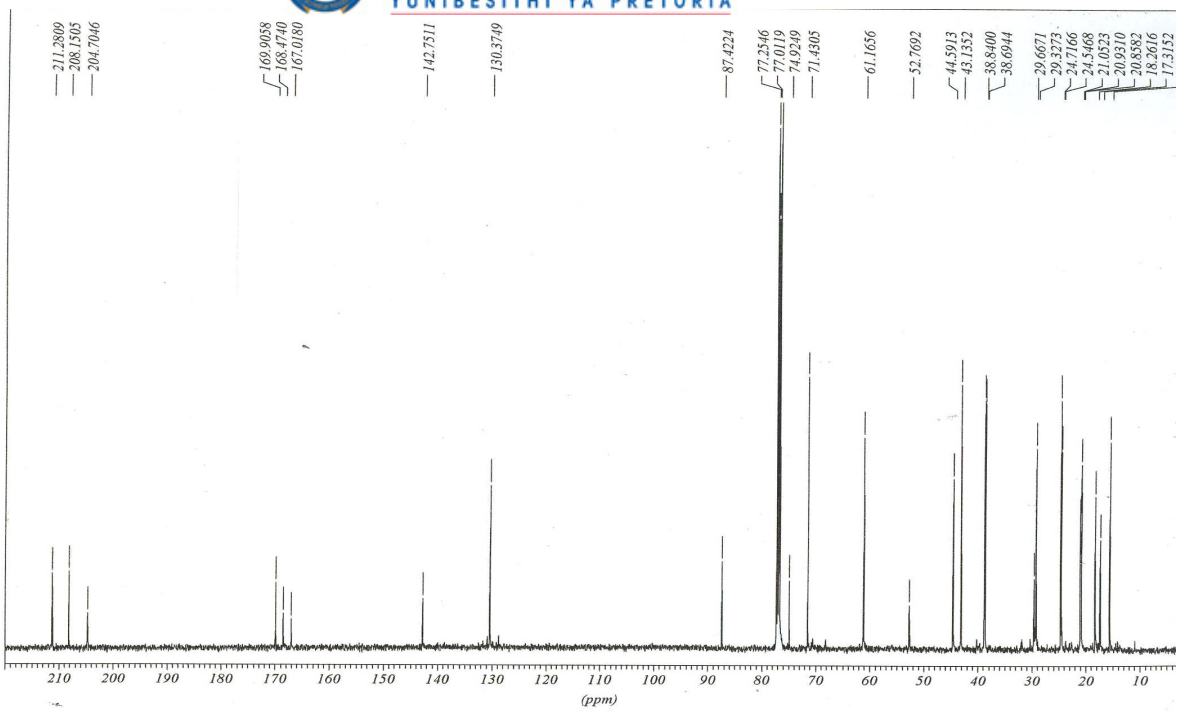

Figure 2.30: ^{13}C-NMR spectrum of steenkrotin B acetate.

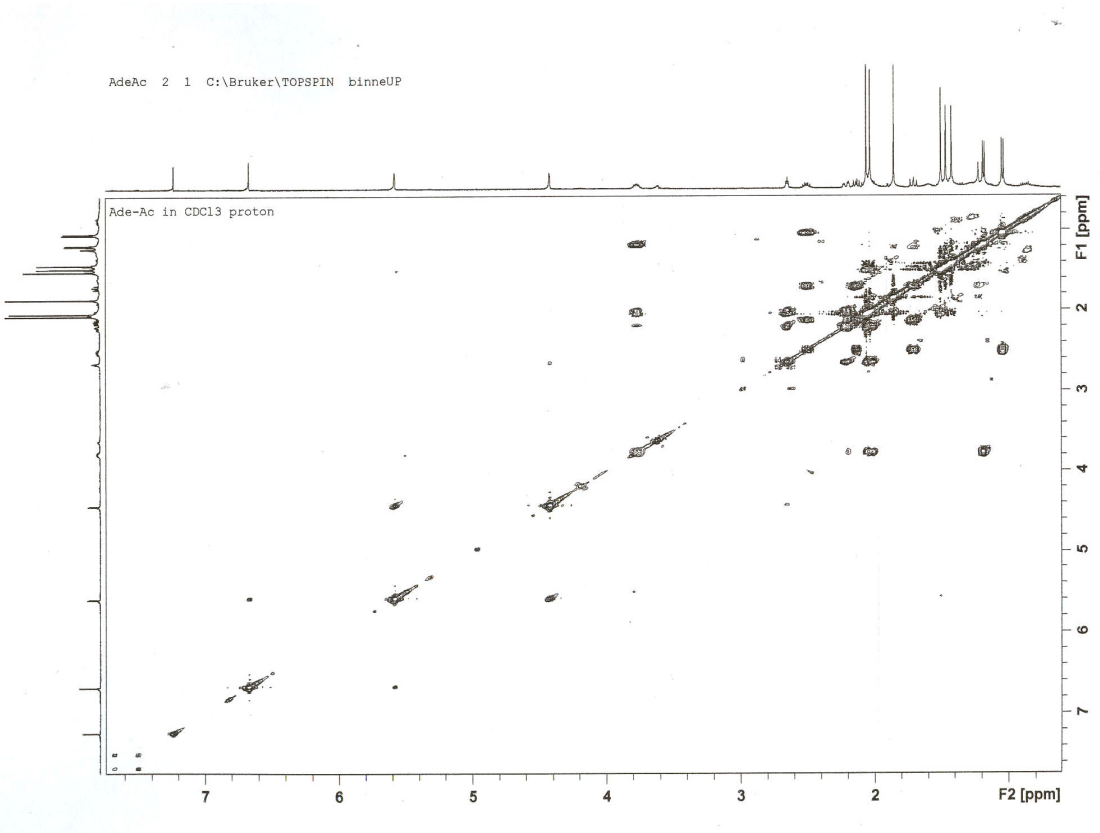

Figure 2.31: COSY spectrum of steenkrotin B acetate.

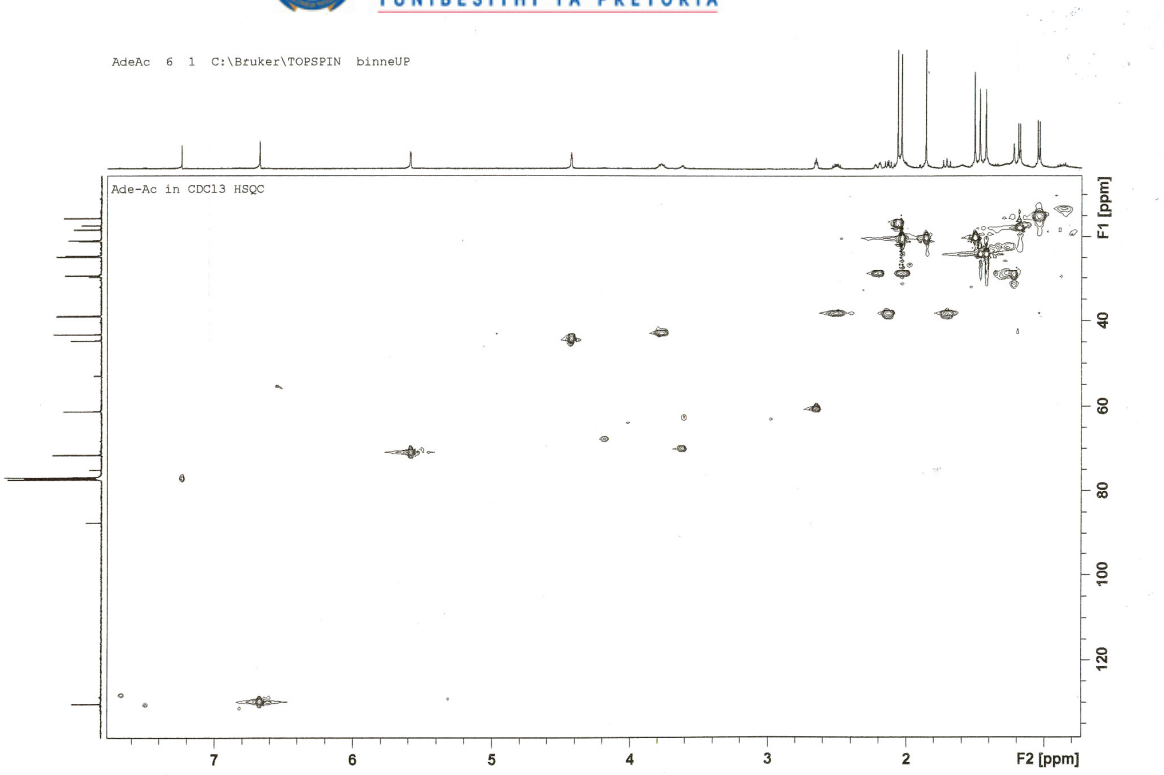

Figure 2.32: HSQC spectrum of steenkrotin B acetate.

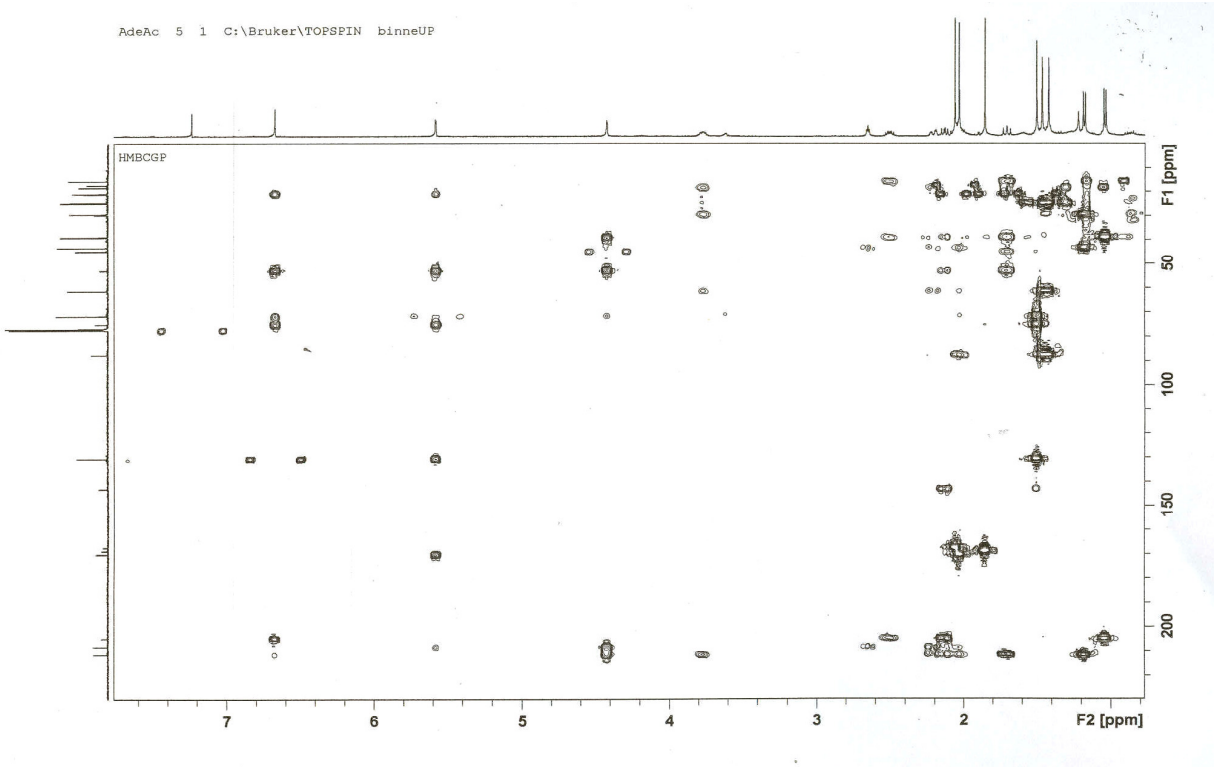

Figure 2.33: HMBC spectrum of steenkrotin B acetate.

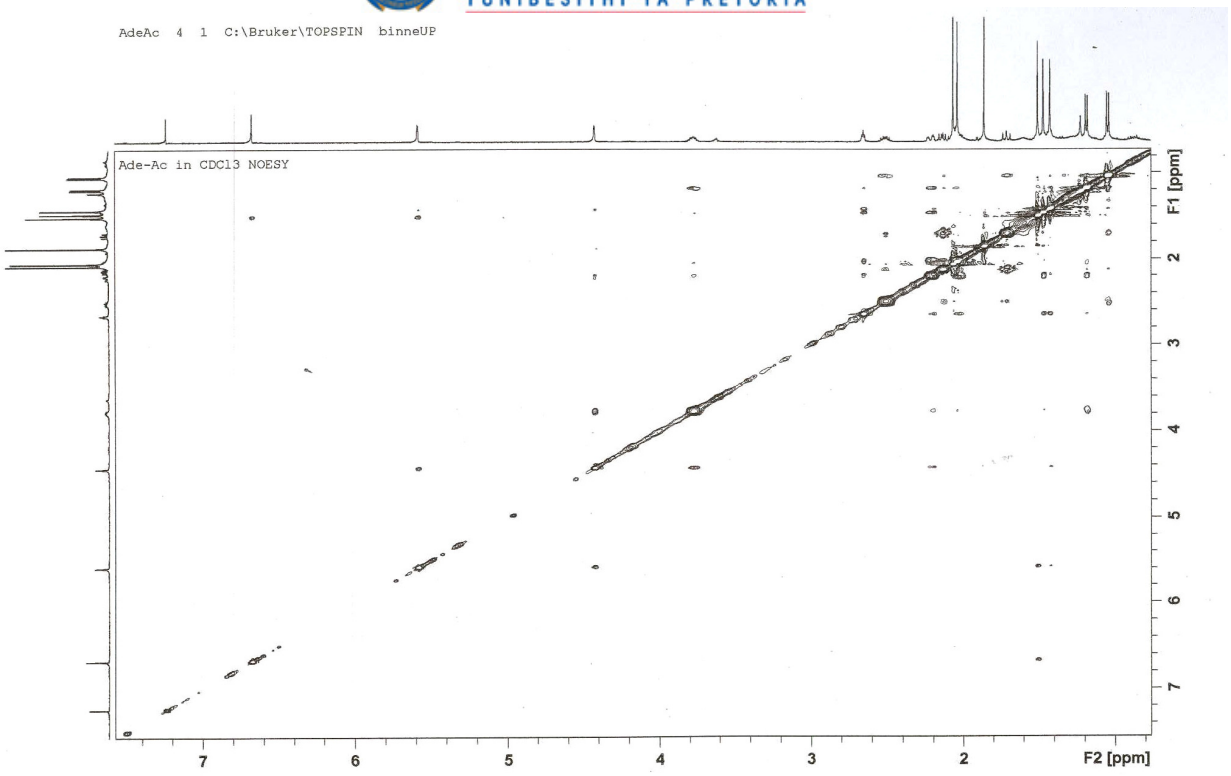

Figure 2.34: NEOSY spectrum of steenkrotin B acetate.

2.4 References:

Baj, S. and Chrobok, A. 2000. Alkylation of peroxyacids as a new method of peroxyester synthesis. J. Chem. Soc., Perkin Trans. *1*:2575-2576.

Boonphong, S., Puangsombat, P., Baramee, A., Mahidol, C., Ruchirawat, S. and Kittakoop, P. 2007. Bioactive compounds from *Bauhinia purpurea* possessing antimalaral, antimycobacterial, antifungal, anti-inflammatory, and cytotoxic activities. J. Nat. Prod. 70:795-801.

Clarkson, C., Maharaj, V.J., Crouch, N.R., Grace, O.M., Pillay, P., Matsabisa, M.G., Bhagwandin, N., Smith P.J., Folb. P.I. 2004. *In vitro* antplasmodial activity of medicinal plants native to or naturalised in South Africa. J. Ethnopharmacol. 92 :177-191.

Eloff, J.N., 1998. A sensitive and quick micro-plate method to determine the minimal inhibitory concentration of plant extract for bacteria. Planta Med. 64 (8):711-713.

Farruggia; L.J. 1997. *ORTEP*-3 for Windows - a version of *ORTEP*-III with a Graphical User Interface (GUI). *J. Appl. Crystallogr*. *30*:565.

Lund, B.M. and Lyon, G.D. 1975. Detection of inhibitors of *Erwina carotovora* and *E. herbicola* on thin layer chromatograms. J. Chromatogr. 110:193-196.

Mercury (Version 1.4.2). 2007. Cambridge Crystallographic Data Centre. URL: http://www.ccdc.cam.ac.uk.

Ngadjui, B.T., Abegaz, B.M., Keumedjio, F., Folefoe, G.N. and Kapche, G.W.F (2002). Diterpenoids from the stem bark of *Croton zambesicus*. Phytochem. 60 (4):345-349.

Noedl, H., Wongsrichanalai C. and Wernsdorfer, W.H. 2003. Malaria drug-sensitivity testing: new assays, new perspectives. Trends Parasitol. 19 (4):175-181.

Olah, G. A.; Parker, D. G.; Yoneda, N. and Pelizza, F. 1976. Oxyfunctionalization of hydrocarbons. 1. Protolytic cleavage-rearrangement of tertiary alkyl hydroperoxides with magic acid. J. Am. Chem. Soc. *98*:2245-2250.

Perales, A.; Martínez-Ripoll, M.; Fayos, J.; Savona, G.; Bruno, M. and Rodríguez, B. 1983. Sesquiterpenoid constituents of *Meriandra benghalensis* (Labiatae). X-ray structure analysis. J. Org. Chem. *48*:5318-5321.

POV-Ray for Windows. (Version 3.6). 2004. Persistence of Vision Raytracer Pty. Ltd., Victoria, Australia. URL: http://www.povray.org.

Prozesky, E.A. 2004. Antiplasmodial and chloroquine resistance reversal properties of a new diterpene from *Croton steenkampianus.* PhD thesis. University of Pretoria, South Africa.

SHELXS-97 and SHELXL-97. Sheldrick, G.M. 1997. University of Gottingen, Germany.

Silver, R.M., Oliveira, F.A., Cunha K.M.A., Maia, J.L., Maciel, M.A.M., Pinto A.C., Nascimento N.R.F., Santos F.A. & Rao V.S.N. (2005). Cardiovascular effects of trans-dehydrocrotonin, a diterpene from *Croton cajucara* in rats. Vascul. Pharmacol. 43(1):11-18.

SMART(Version 5.054), SAINT (Version 6.45), SADABS (Version 2.10) and SHELXTS / SHELXTL (Version 6.12). 2001. Bruker AXS Inc., Madison, Wisconsin, USA. 6.45.

Stoltz, A.C. 1992. Biochemical and immunochemical investigation of some South African strains of the human malaria parasite, *Plasmodium falciparum*. MSc thesis, University of Pretoria, Pretoria, South Africa.

Suarez, A.I., Blanco Z., Compagnone R.S., Salazar-Bookaman M.M., Zapata V., Alvarado C. (2006). Anti-inflammatory activity of *Croton cuneatus* aqueous extract. J. Ethnopharmacol. 105:99-101.

Suarez, A.I., Compagnone R.S., Salazar-Bookaman M.M., Tillett S., Monache F.D., Giulio C.D. and Bruges G. 2003. Antinociceptive and anti-inflammatory effects of *Croton malambo* bark aqueous extract. J. Ethnopharmacol. 88 (1):11-14.

Trager, M. and Jensen, J.B. 1976. Human malaria parasite in continuous culture. Science 193:674.

Willcox, M.L. and Bodeker, G. 2004. Traditional herbal medicines for malaria. B.M.J. 329:1156-1159.

Zdzislawa, N. 2007. A review of anti-infective and anti-inflammatory chalcones. Eur. J. Med. Chem. 42(2):125-137.